Oil & Natural Gas Technology

DOE Award No.: DE-FC26-05NT15457

Final Report

Reporting Period Start Date: October 2005
Reporting Period End Date: March 2008

Rapid Calibration of High Resolution Geologic Models to Dynamic Data Using Inverse Modeling: Field Application and Validation

Submitted by:
Texas Engineering Experiment Station
Texas A&M University, College Station, TX

Prepared for:
United States Department of Energy
National Energy Technology Laboratory

June, 2008

Office of Fossil Energy

Title Page

Rapid Calibration of High Resolution Geologic Models to Dynamic Data Using Inverse Modeling: Field Application and Validation

FINAL REPORT

Reporting Period Start Date: October 2005
Reporting Period End Date: March 2008

Principal Author: Akhil Datta-Gupta
June, 2008

DOE Contract No. DE-FC26-05NT15457

Submitting Organization:
Texas Engineering Experiment Station
Texas A&M University, College Station, TX

Subcontractor: D. W. Vasco
Lawrence Berkeley National Laboratory
Berkeley, CA

DISCLAIMER

ABSTRACT

Streamline-based assisted and automatic history matching techniques have shown great potential in reconciling high resolution geologic models to production data. However, a major drawback of these approaches has been incompressibility or slight compressibility assumptions that have limited applications to two-phase water-oil displacements only. We propose an approach to history matching three-phase flow using a novel compressible streamline formulation and streamline-derived analytic sensitivities. First, we utilize a generalized streamline model to account for compressible flow by introducing an "effective density" of total fluids along streamlines. Second, we analytically compute parameter sensitivities that define the relationship between the reservoir properties and the production response, viz. water-cut and gas/oil ratio (GOR). These sensitivities are an integral part of history matching, and streamline models permit efficient computation of these sensitivities through a single flow simulation. We calibrate geologic models to production data by matching the water-cut and gas/oil ratio using our previously proposed generalized travel time inversion (GTTI) technique. For field applications, however, the highly non-monotonic profile of the gas/oil ratio data often presents a challenge to this technique. In this work we present a transformation of the field production data that makes it more amenable to GTTI. Further, we generalize the approach to incorporate bottom-hole flowing pressure during three-phase history matching. We examine the practical feasibility of the method using a field-scale synthetic example (SPE-9 comparative study) and a field application.

Recently Ensemble Kalman Filtering (EnKF) has gained increased attention for history matching and continuous reservoir model updating using data from permanent downhole sensors. It is a sequential Monte-Carlo approach that works with an ensemble of reservoir models. Specifically, the method utilizes cross-covariances between measurements and model parameters estimated from the ensemble. For practical field applications, the ensemble size needs to be kept small for computational efficiency. However, this leads to poor approximations of the cross-covariance matrix, resulting in loss of geologic realism. Specifically, the updated parameter field tends to become scattered with a loss of connectivities of extreme values such as high permeability channels and low permeability barriers, which are of special significance during reservoir characterization. We propose a novel approach to overcome this limitation of the EnKF through a 'covariance localization' method that utilizes sensitivities that quantify the influence of model parameters on the observed data. These sensitivities are used in the EnKF to modify the cross-covariance matrix in order to reduce unwanted influences of distant observation points on model parameter updates. The key to the success of the sensitivity-based covariance-localization is its close link to the underlying physics of flow compared to a simple distance-dependent covariance function as used in the past. This flow-relevant conditioning leads to an efficient and robust approach for history matching and continuous reservoir model updating, avoiding much of the problems in traditional EnKF associated with instabilities, parameter overshoots and loss of geologic continuity. We illustrate the power and utility of our approach using both synthetic and field applications.

TABLE OF CONTENTS

EXECUTIVE SUMMARY

Available information on subsurface heterogeneity can be broadly categorized into two major types: static and dynamic. Static data are time-invariant direct or indirect measurements of reservoir properties, such as cores, well logs, and 3-D seismic data. With recent advances in reservoir characterization, these data can now be integrated efficiently into coherent 3-D reservoir descriptions. Dynamic data are the time dependent measurements of flow responses such as pressure, flow rate, fractional flow and, with the use of 4-D seismic, time-lapse saturation and pressure. Geological models derived from static data alone often fail to reproduce the dynamic response from petroleum reservoirs. Reconciling geologic models to the dynamic response of the reservoir is critical for subsurface characterization and building reliable reservoir performance models. Integration of dynamic data generally leads to an inverse problem and requires solution of the flow equations several times using an iterative procedure. The process is commonly referred to as "history matching" and is usually the most tedious and time-consuming aspect of subsurface flow and transport simulation study.

Recently streamline models have shown great promise in history matching high resolution geologic models. Streamline models decompose the three-dimensional simulation into a series of 1-D simulations that are decoupled from each other and can be solved very efficiently. In spite of its significant potential, a major drawback of the streamline-based approaches has been the inability to include complex physics and incompressibility or slight compressibility assumptions that have limited applications primarily to two-phase water-oil displacements. In this work, we generalize streamline models to compressible flow using a rigorous formulation while retaining most its computational advantages. Next, we generalize the streamline-based history matching to compressible and three-phase flow including water, oil and gas phases. As a result of this work, streamline-based history matching can now be applied to a much wider class of reservoirs, including oil reservoirs below bubble point pressure and in the presence of three-phase flow.

With the advent of smart well and permanent downhole sensors, the petroleum industry is now able to collect data such as pressure and rate data, on a continuous basis. This has resulted in the need for methods for continuous model updating, much along the line of weather forecasting. The goal is to keep the models 'live' and updated as and when the data becomes available. This is in contrast to the current practice of history matching which is carried out only in the intervals of a few years, mainly because of the computation time and manpower involved. In this work, we explore the use of proven techniques from weather forecasting viz. Ensemble Kalman Filters (EnKF) for continuous model updating. It is a sequential Monte-Carlo approach that works with an ensemble of reservoir models. Specifically, we propose a flow-relevant conditioning of EnKF that leads to an efficient and robust approach for history matching and continuous reservoir model updating, avoiding much of the problems in traditional EnKF associated with instabilities, parameter overshoots and loss of geologic continuity. We illustrate the power and utility of our approach using both synthetic and field applications. The field case is from the Gold Smith San

Andres Unit GSAU, a dolomite formation in west Texas. The CO2 injection pilot area consists of nine inverted five-spot patterns covering approximately 320 acres with an average thickness of 100 ft. The area has 20 years of waterflood production history before the initiation of the CO2 project in 1996. The study area includes 11 injectors and 31 producers. Production history information from 9 producers is used because only these have significant water cut response. The field application clearly demonstrates the ability of our approach in assimilating production history continuously while preserving geologic realism.

This final report is divided into two major parts that describes the major results and accomplishments from this project. The following papers were published based on the work from this research project.

- Datta-Gupta, A., Devegowda, D., Oyerinde, D. and Cheng, H., "The Role of Streamline Models for Data Assimilation in Petroleum Engineering and Hydrogeology," in Quantitative Information Fusion for Hydrological Sciences, Eds. Xing Cai and T.-C. Jim Yeh, Springer Verlag Publishers (2007).
- Cheng, H., Oyerinde, D., Datta-Gupta, A. and Milliken, W. "Compressible Streamlines and Three-phase History Matching," SPE Journal, 12(4), (December 2007).
- Oyerinde, Adedayo., Datta-Gupta, A., and Milliken, W., "Experiences With Streamline-Based Three-phase History Matching," SPE 109964 presented at the 2007 SPE Annual Technical Conference and Exhibition, Anaheim, CA, U.S.A., 11–14 November 2007.
- Devegowda Deepak, Arroyo, Elkin and Datta-Gupta, A., "Efficient and Robust Reservoir Model Updating Using Ensemble Kalman Filter With Sensitivity Based Covariance Localization," SPE 106144 to be presented at the SPE Reservoir Simulation Symposium, Houston, TX, 26-28 February, 2007.(to appear in SPEREE)
- Elkin Arroyo-Negrete, Deepak Devegowda, Akhil Datta-Gupta, "Streamline-Assisted Ensemble Kalman Filter for Rapid and Continuous Reservoir Model Updating," SPE 104255 presented at the 2006 SPE International Oil & Gas Conference and Exhibition in China held in Beijing, China, 5–7 December 2006

EXPERIMENTAL

No experiments were performed at Texas A&M during the project.

RESULTS AND DISCUSSION: INTRODUCTION

This research concerns history matching of high resolution geologic models consisting of hundreds of thousands to million-cell models in an efficient manner for improved performance predicitons of petroleum reservoirs. The work consists of two major parts which are briefly introduced below. More detailed discussion on each part follows the introduction.

In the first part, we propose a method to improve the current work flow of history matching. The traditional history matching approach generally involves periodically (once in a few years) updating geolgic models based on the avialable production data upto that point in time. It frequently uses local or regional multipliers of pore volumes and transmissibilities to modify the reservoir properties. By adjusting the regions and multipliers, a history match can often be achieved using trial and error. Such trial-and-error involves considerable subjective judgment and personal bias, and very often creates artificial discontinuities with loss of geologic realism. Automatic history matching or production data integration methods utilize inverse theory to minimize an appropriately defined misfit function to obtain a history match. Formally, this class of inverse problems is known as ill-posed, and must be managed (regularized), e.g., by constraining the solution to independent prior information. In our previous works we have shown that streamline models offer some unique advantages in automatic history matching. In this work, we build upon our previous success with streamline-based history matching to generalize the approach to handle a much wider class of reservoirs without any perceptible loss in speed and accuracy. Specifically, we generalize the streamline approach to compressible flow and extend streamline-based history matching to three-phase flow in the presence of free gas. Our approach will lead to significant savings in computation time and man power compared to the conventioanl history matching magnitude faster than conventional

In the second part of the work, we explore new and evolving concepts in history matching viz. sequential updating of reservoir models based on data from permanent downhole sensors. The goal here is to update geologic models with production data as and when the data becomes available. Such continuous reservoir model updating is much along the line of weather forecasting and we explore the use of proven methods in weather forecasting viz. the Ensemble Kalman Filter (EnKF). The EnKF is a Monte-Carlo approach that works with an ensemble of reservoir models. Specifically, the method quantifies the relationship between reservoir parameters and production data using cross-covariances between measurements and model parameters computed directly from the ensemble members. This information is then used to sequentially update the reservoir models. For practical field applications, the ensemble size needs to be kept small for computational efficiency. However, this leads to poor approximations of the cross-covariance matrix and loss of geologic realism. In this work we propose a novel streamline-assisted EnKF that is quite general and avoids much of the problems in the traditional EnKF associated with instabilities, overshooting and loss of geologic continuity during model updating. Our approach leads to a systematic approach to sequentially update high resolution geologic models using dynamic data in a ‘near real time’ fashion. In this way, we can keep geologic models ‘live’ with respect to all static and dynamic information which will facilitate decision making in a very significant way.

RESULTS AND DISCUSSION: PART I

Development and Field Experiences With Streamline-Based Three-phase History Matching

Geologic models derived from static data alone typically fail to reproduce the production history of a reservoir. It is important to reconcile simulation models to the dynamic response of the reservoir, i.e., the production history. This necessity has been the motivation behind the active research work in history matching. Traditionally, history matching is performed manually by applying local and regional changes to reservoir properties. While this is still in general practice, the subjective overtone of this approach, the time and manpower requirements, and the potential loss of geologic consistency have led to the development of a variety of alternative workflows for assisted and automatic history matching. Automatic history matching requires the solution of an inverse problem by minimizing an appropriately defined misfit function.[1-8] The objective function is usually formulated so as to match the production history and at the same time preserve geologic realism in the history matched models.

Recent advances in geostatistics have led to the building of high-resolution geologic models consisting of millions of cells. Most of these are scaled up to the sub-million size for reservoir simulation purposes. History matching even the scaled up models is computationally prohibitive. The associated cost in terms of time and manpower has led to increased interest in efficient history matching techniques and in particular, to sensitivity-based algorithms because of their rapid convergence. Furthermore, of the sensitivity-based methods, streamline-based production data integration has proven to be extremely efficient computationally.[2]

The computational efficiency of the streamline method as a 'forward-model' has historically been its major appeal to the petroleum industry. More recently, attention has been drawn to streamline simulation because of its rapid model calibration capability; specifically, the ability to calculate sensitivity coefficients using only a single forward simulation. The recent extension of the streamline formulation to account for compressibility has extended its applicability. This has also been the motivation behind the generalization of its inverse modeling capability to three phase flow data.[9] In this work, using streamline-derived sensitivities, we examine the practical feasibility of the approach by applying it to both synthetic and field cases.

For history matching, we use a previously proposed generalized travel-time inversion (GTTI) technique that has been successfully applied to many field cases involving two-phase flow.[10] Our work here generalizes the approach to three phase flow by incorporating matching of water-cut, gas oil ratio and the flowing bottom-hole pressure at the producing wells. The highly non-monotonic profile of the field observed gas/oil ratio data, together with measurement inaccuracies can be a challenge for field-scale history matching of three-phase flow using GTTI. The approach to history matching presented here requires the transformation of observed production data to composite quantities. This transformation of data helps us circumvent some of the difficulties. In particular, our proposed transformation leads to production profiles that are more amenable to misfit computations via the generalized travel time technique. We also show the need and importance of matching the bottom-hole pressure during history matching three-phase flow.

The outline of our report is as follows. First, we discuss the basic steps in our proposed approach and illustrate the history matching procedure using a synthetic example. Next, we describe the streamline formulation for compressible and three-phase flow. We discuss the data transformation and the mathematical formulation of the analytical sensitivities for water-cut and gas/oil ratio during compressible and three-phase flow and also, the semi-analytic representation of the BHP sensitivity. Finally, we present field examples to demonstrate the practical feasibility of our method.

Basic Steps of the Approach

The main steps of the approach to three-phase history matching discussed in this work are as follows:

- **Three-phase Flow Simulation**. We use a 3-D compressible streamline simulator for modeling three-phase flow in the reservoir and to obtain the water-cut, GOR and bottom-hole flowing pressure response. However, the history matching approach presented here can be applied to finite-difference simulations also provided streamlines and time of flight are computed based on the finite-difference velocity field at the required time intervals.

- **Data Misfit via Generalized Travel Time.** Production data misfit is represented by a 'generalized travel time' at each producing well.[10] A 'generalized travel time' or 'travel time shift' is computed by systematically shifting the computed production response towards the observed data until the cross-correlation between the two is maximized. The approach preserves the robustness of a travel time inversion and improves computational efficiency by representing the production data misfit at a well in terms of a single 'travel time shift'.

- **Sensitivity Computations and Data Inversion.** In the presented approach, we compute the arrival time sensitivity of composite saturation quantities to reservoir parameters as opposed to the arrival time sensitivity of water-cut and GOR to a reservoir parameter. The sensitivity is computed as 1-D integrals along the trajectory of a streamline. The sensitivity of the bottom-hole flowing pressure is computed using a low frequency asymptotic approach.[11] Production history matching is performed via a generalized travel time inversion that minimizes 'travel time shifts' at the producing wells.[10] An iterative least-squared minimization technique that utilizes the analytic sensitivity coefficients is used for this purpose.[12] Additional constraints are imposed using a prior model to reduce non-uniqueness in the solution and also to preserve geologic realism.

- **Data Transformation.** Consistent with the sensitivity computation, we transform the production history (water-cut, and gas/oil ratio) to the equivalent saturation quantities for misfit computation via the generalized travel-time technique. The generalized travel-time technique is particularly effective when the field production history is nearly monotonic as it is the case for a typical water-cut profile. The same cannot be said about the gas/oil ratio data. Because of its highly non-monotonic nature, the GOR data can become a challenge for computation of data misfit using the generalized travel time technique. Our

experience shows that the transformation of the production history to composite quantities that are functions of well block pressure and saturation makes the production response more amenable to generalized travel time computations. This transformation is carried out on both the observed and simulated response and the misfit is then quantified in terms of travel-time difference in the transformed data space

Before discussing the mathematical details, we first illustrate the procedure using a synthetic example described below.

A Synthetic Example: This synthetic case is a nine-spot model and involves reconstructing a reference permeability field by the simultaneous integration of three-phase production data. The reference permeability distribution is shown in **Fig.1a**. The mesh size used is 21×21×1. The reference permeability distribution consists of a north trending low-permeability feature and a high-permeability trend towards the south. To perform the history match, we first transform the water-cut and GOR data to the composite quantities in a manner described later. **Figs 2a&b** show the match of the transformed quantities while **Figs 2c&d** show the match of the water-cut and gas/oil ratio data. In this case, the transformation not only retains the monotonic profile of the water-cut data, the non-monotonic gas-oil ratio data also becomes monotonic, making it suitable for the generalized travel time computations. The resulting permeability distribution shown in **Fig.1b** captures the general trend of the reference permeability field. The convergence of the inversion is shown in **Fig. 3** where all the misfit indices are shown to have dropped to about ten percent of their initial value in just six iterations. The ten iterations shown only took about 8 minutes on a PC (Intel Xeon 3.06 GHz Processor)

Fig. 2e compares the bottom hole flowing pressure (BHP) for the reference case to the well flowing pressure in the wells at the final iteration. It is obvious that while we have an acceptable match on the production data viz. water cut and GOR, we have not been able to adequately reproduce the reservoir energy. Next, we perform a simultaneous integration of water-cut, gas/oil ratio, and the bottom-hole pressure. The BHP sensitivity coefficients that relate perturbations in reservoir permeability to perturbations in pressure observations are obtained using a low-frequency asymptotic method.[11] The matching of the bottom-hole pressure is carried out in the frequency domain by taking a Fourier transform of the BHP data. In our application, we have incorporated only the zero frequency expression of the zero-order expansion of the asymptotic solution to preserve computational efficiency. This is equivalent to matching static pressures only at the well.

Fig.4 shows the match resulting from this inversion. For the same number of iterations, the match of water-cut and GOR somewhat deteriorates as compared to **Fig.2** partly because the inversion is now more constrained. This trade-off, however, results in a better match of the reservoir energy as shown by the BHP match of the wells (contrast **Figs.2e and 4e**). Note that although we have limited to matching the zero frequency component only, we still obtain a reasonable match to the BHP response over all times for this case. The importance of matching the BHP will become clear as we discuss the mathematical formulation in the next section.

Mathematical Formulation

The advantage of streamline-based dynamic data integration is a direct consequence of the efficiency with which the parameter 'sensitivities' are calculated. The primary basis of these sensitivities is the streamline formulation, generalized for compressible three-phase flow. For

this reason, we first highlight the important features of this compressible formulation, thus paving the way for a thorough discussion of the derivation of the analytical sensitivities.

Effective Density and Compressible Streamlines. In 3-D, streamlines are defined by the intersection of two bi-streamfunctions, ψ and χ. For compressible three-phase flow in porous media, the conserved quantity is a total multi-phase mass flux. Accordingly, the bi-streamfunctions are defined to incorporate the compressibility effects.[13]

$$\rho\vec{u} = \nabla\psi \times \nabla\chi \quad \text{.....(1a)}$$

where ρ represents an 'effective density' of the total fluid. Since $\rho\vec{u}$ represents a conserved flux.

$$0 = \nabla \bullet (\nabla\psi \times \nabla\chi) = \nabla \bullet (\rho\vec{u}) \\ = \vec{u} \bullet \nabla\rho + \rho\nabla \bullet \vec{u} \quad \text{. .....(1b)}$$

In streamline simulation, we work in the time of flight coordinates rather than the physical space. This coordinate change is characterized by the Jacobian of transformation.

$$\left\| \frac{\partial(\tau, \psi, \chi)}{\partial(x, y, z)} \right\| = (\nabla\psi \times \nabla\chi) \bullet \nabla\tau = \rho\vec{u} \bullet \nabla\tau = \rho\phi \quad \text{.... (2)}$$

Eq.2 shows that the operator identity $u \bullet \nabla = \phi \frac{\partial}{\partial\tau}$ used for incompressible streamline formulation holds good for compressible flow also. Applying the identity to **Eq.1b** gives the ordinary differential equation below.

$$\phi \frac{\partial\rho}{\partial\tau} + \rho\nabla \bullet \vec{u} = 0 \cdot \text{ ..... (3)}$$

where the divergence of flux $\nabla \bullet \vec{u}$ is a constant within each grid cell but varies spatially along the streamlines from cell to cell. Integrating **Eq.3** permits the evaluation of the effective density along the streamlines starting with a value of unity at the injectors.

$$\rho = \rho_0 e^{-\left(c\frac{\tau}{\phi}\right)} \quad \text{..... (4)}$$

With the initial volumetric flux $\Delta Q = \Delta\psi\,\Delta\chi$ being assigned to a streamline, the volumetric flux will vary along the streamline according to the relationship $\frac{1}{\rho}\Delta Q$.

Three phase Black Oil Simulation. The mass conservation equation for the water phase is given by **Eq. 5**

$$\phi \frac{\partial}{\partial t}\left(\frac{S_w}{B_w}\right) + \nabla \cdot \left(\frac{f_w \vec{u}}{B_w}\right) = 0 \quad \text{.....(5)}$$

$$\phi \frac{\partial}{\partial t}\left(\frac{S_w}{B_w}\right) + \frac{f_w}{B_w}\nabla \cdot \vec{u}_t + \vec{u}_t \cdot \nabla\left(\frac{f_w}{B_w}\right) = 0 \quad \text{.....(6)}$$

Transforming to the streamline time of flight coordinate and noting that $\nabla \bullet \vec{u} = c$ gives,

$$\phi \frac{\partial}{\partial t}\left(\frac{S_w}{B_w}\right) + \phi \frac{\partial}{\partial\tau}\left(\frac{f_w}{B_w}\right) = -\frac{f_w}{B_w} c \quad \text{.....(7)}$$

$$\frac{\partial}{\partial t}\left(\frac{S_w}{B_w}\right)+\frac{\partial}{\partial \tau}\left(\frac{f_w}{B_w}\right)=-\frac{c}{\phi}\frac{f_w}{B_w} \quad \text{.....(8)}$$

The right hand side in **Eq. 8** can be seen as a compressibility-induced source term attributable to fluid compression and expansion. For incompressible flow, $c = 0$ everywhere and the right hand term vanishes.

The gas saturation equation along streamlines can be obtained following the same procedure as the water phase starting with the mass conservation equation for the gas,

$$\phi\frac{\partial}{\partial t}\left(\frac{S_g}{B_g}+\frac{S_oR_s}{B_o}\right)+\nabla\cdot\left(\vec{u}_t\frac{f_g}{B_g}+\vec{u}_t\frac{f_oR_s}{B_o}\right)=0 \quad \text{.....(9)}$$

After transforming to streamline time of flight coordinate, we get the following 1-D equation along streamlines,

$$\frac{\partial}{\partial t}\left(\frac{S_g}{B_g}+\frac{S_oR_s}{B_o}\right)+\frac{\partial}{\partial \tau}\left(\frac{f_g}{B_g}+\frac{f_oR_s}{B_o}\right)=-\left(\frac{f_g}{B_g}+\frac{f_oR_s}{B_o}\right)\frac{c}{\phi} \qquad (10)$$

Sensitivity Calculation for Compressible and Three-Phase Flow. In reconciling simulation models to dynamic data, we aim at minimizing the vertical (amplitude) difference between the observed and calculated production profiles at each observation time by adjusting reservoir parameters. Formulating the sensitivities accordingly results in what is termed an 'amplitude match'. Alternatively, since production response is characterized by well node saturation/saturations, matching at each observation time the saturation/saturations characterizing production achieves the same purpose. In essence, the aim is to match the 'arrival' time of the characteristic saturation/saturations. This approach is termed a 'travel-time' match. In our approach, we avoid the traditional amplitude match because of its high non-linearity and we quantify data misfit in terms of travel-time. The central idea in the sensitivity computation is that for a fixed pressure, a given saturation (two-phase flow) or combination of saturations (three-phase flow) uniquely determines a production response such as water-cut or gas/oil ratio. Thus, instead of computing the reservoir parameter sensitivity to a particular observed water-cut for instance, we compute the sensitivity of the arrival time of the saturation (two-phase flow) or saturations (three-phase flow) that characterize the water-cut observation. Clearly, for incompressible two-phase oil-water application, a given water saturation uniquely determines the fractional flow to water and thus, water-cut. In the case of three-phase flow the situation is more complicated even for incompressible flow. However, in general for a fixed pressure a given combination of water-cut and gas/oil ratio gives a unique combination of saturation (i.e. sg, and sw) and vice versa. This is illustrated in **Fig. 5** where we have plotted truncated families of gas and water saturation variation with gas/oil ratio and water-cut at a fixed pressure. We can see that the intersection of a horizontal and vertical line on bottom plot of **Fig 5** uniquely determines a saturation pair. This emphasizes the need for a simultaneous assimilation of BHP, gas/oil ratio and water-cut data. For a given pressure, a simultaneous match of gas/oil ratio and water-cut is equivalent to a simultaneous match of the composite quantities S_w/B_w and $S_g/B_g + S_oR_s/B_o$ denoted

as S_w' and S_g' respectively. It is the arrival-time sensitivity of these composite quantities that we are interested in.

Water Saturation Arrival Sensitivity. To motivate the derivation for compressible flow, we briefly consider the incompressible flow case. The saturation velocity for a given saturation contour S_w along a streamline will be given by,

$$\left.\frac{\partial \tau}{\partial t}\right|_{S_w} = \left.\frac{df_w}{dS_w}\right|_{S_w} \quad \text{.....(11)}$$

This follows from the incompressible water saturation equation**.** The arrival time of the saturation front will be,

$$t|_{Sw} = \tau \Big/ \left.\frac{df_w}{dS_w}\right|_{S_w} \quad \text{.....(12)}$$

In our previous work, we used the above relationship to compute the sensitivity of the arrival time of the saturation front based on the sensitivity of the time of flight to a perturbation in the reservoir parameter.[1, 10] Specifically, the sensitivity of the saturation arrival time with respect to reservoir parameter m is computed as,

$$\left.\frac{\partial t}{\partial m}\right|_{S_w} = \frac{\dfrac{\partial \tau}{\partial m}}{\left.\dfrac{df_w}{dS_w}\right|_{S_w}} \quad \text{.....(13)}$$

where the sensitivity of the time of flight is computed analytically from streamline simulation.

We can generalize the sensitivity calculations using the saturation equation for compressible flow along a streamline, **Eq. 8** which can be rearranged as follows,

$$\frac{\partial}{\partial t}\left(\frac{S_w}{B_w}\right) = -\frac{\partial}{\partial \tau}\left(\frac{f_w}{B_w}\right) - \frac{c}{\phi}\frac{f_w}{B_w} \quad \text{..... (14)}$$

In generalized travel time inversion of production data, we are interested in obtaining the partial derivative of the arrival time of saturation with respect to reservoir parameters, m for example permeability.[1] Let $S_w^{'}$ represent the quantity S_w / B_w in the water saturation equation. For a given pressure, $S_w^{'}$ is functionally dependent on t (the arrival time) and τ (the time of flight) which in turn depend on m. For a fixed $S_w^{'}$, we can express this implicitly as follows,

$$\frac{\partial S_w^{'}}{\partial t}\frac{\partial t}{\partial m} + \frac{\partial S_w^{'}}{\partial \tau}\frac{\partial \tau}{\partial m} = 0 \quad \text{..... (15)}$$

A simple manipulation of **Eq. 15** shows that

$$\left.\frac{\partial t}{\partial m}\right|_{S_w^{'}} = -\frac{\dfrac{\partial S_w^{'}}{\partial \tau}\dfrac{\partial \tau}{\partial m}}{\dfrac{\partial S_w^{'}}{\partial t}} \quad \text{..... (16)}$$

Substituting **Eq.8** for the denominator gives the required travel time sensitivity for a fixed S_w'.

$$\left.\frac{\partial t}{\partial m}\right|_{S_w'} = \frac{\frac{\partial S_w'}{\partial \tau}\frac{\partial \tau}{\partial m}}{\frac{\partial}{\partial \tau}\left(\frac{f_w}{B_w}\right)+\frac{f_w}{B_w}\frac{c}{\phi}} \quad \text{..... (17)}$$

For incompressible flow, $c = 0$, B_w is constant and **Eq. 17** reduces to the familiar formulation for incompressible flow.[10] All the terms in **Eq. 17** can be computed along the streamline. Specifically, $\partial\tau/\partial m$ is computed analytically under the assumption that the streamlines do not shift because of small perturbation in reservoir properties.[1] The remaining partial derivatives are approximated by a backward difference along the streamline.

Gas Saturation Arrival Sensitivity. The conservation equation for gas is given in **Eq. 10**. Let S_g' represent the quantity $S_g/B_g + S_oR_s/B_o$, we rewrite **Eq. 10** in the form below

$$\frac{\partial S_g'}{\partial t} = -\frac{\partial}{\partial \tau}\left(\frac{f_g}{B_g}+\frac{f_oR_s}{B_o}\right)-\left(\frac{f_g}{B_g}+\frac{f_oR_s}{B_o}\right)\frac{c}{\phi} \quad \text{..... (18)}$$

For a given pressure, S_g' depends on t (the arrival time) and τ (the time of flight). For a fixed S_g', we can express this dependence implicitly as follows,

$$\frac{\partial S_g'}{\partial t}\frac{\partial t}{\partial m}+\frac{\partial S_g'}{\partial \tau}\frac{\partial \tau}{\partial m}=0 \quad \text{..... (19)}$$

$$\left.\frac{\partial t}{\partial m}\right|_{S_g'} = -\frac{\frac{\partial S_g'}{\partial \tau}\frac{\partial \tau}{\partial m}}{\frac{\partial S_g'}{\partial t}} \quad \text{..... (20)}$$

Substituting **Eq. 18** for the denominator gives the travel-time sensitivity to a fixed S_g'.

$$\left.\frac{\partial t}{\partial m}\right|_{S_g'} = \frac{\frac{\partial S_g'}{\partial \tau}\frac{\partial \tau}{\partial m}}{\frac{\partial}{\partial \tau}\left(\frac{f_g}{B_g}+\frac{f_oR_s}{B_o}\right)+\left(\frac{f_g}{B_g}+\frac{f_oR_s}{B_o}\right)\frac{c}{\phi}} \quad \text{..... (21)}$$

$$\left.\frac{\partial t}{\partial m}\right|_{S_g'} = \frac{\frac{\partial}{\partial \tau}\left(\frac{S_g}{B_g}+\frac{S_oR_s}{B_o}\right)\frac{\partial \tau}{\partial m}}{\frac{\partial}{\partial \tau}\left(\frac{f_g}{B_g}+\frac{f_oR_s}{B_o}\right)+\left(\frac{f_g}{B_g}+\frac{f_oR_s}{B_o}\right)\frac{c}{\phi}} \quad \text{..... (22)}$$

Again, the parameters needed to compute the partial derivatives are readily available along streamlines.

It is important to note that our sensitivity derivations have not explicitly accounted for the pressure effects. In fact, we can uniquely define S_w' and S_g' based on the water-cut and GOR only at a fixed pressure. Thus, it is critical to match the BHP along with the water-cut and GOR data.

Sensitivity Calculations for the BHP. We carry out matching of the pressure data in the frequency domain following the procedure outlined by Vasco and Karasaki.[11] We take a Fourier transform of the bottom-hole pressure data and match only the zero-th frequency component of

the data. This actually corresponds to matching the static pressure at the wells only. As shown with the synthetic examples, matching simultaneously the zero-th frequency component of the pressure data along with the composite saturation quantities result in a reasonable match of the water-cut, GOR, and bottom-hole pressure data. After Vasco and Karasaki, the sensitivity coefficients for the zero-th frequency (ω=0) is given by

$$\frac{\partial \hat{P}(x, w=0)}{\partial k(y)} = -2\nabla P_o(x|y).\nabla P_o(x_s|y)\Psi^2(\omega) \quad \text{..... (23)}$$

where $P_o(x|y)$ signifies the zero-th order pressure amplitude at the point ***y*** due to a source at ***x***, and $P_o(x_s|y)$, the pressure amplitude at point ***y*** due to a source at point $\boldsymbol{x}_{\boldsymbol{s}}$. The term $\Psi^2(\omega)$ accounts for rate variations and widowing in time. The readers are referred to the original paper for more details. To compute the sensitivity using **Eq. 23**, the zero-th order pressure amplitudes are obtained from the equivalent steady state solutions of the original problem. Since this approach requires steady-state solutions, it is computationally more attractive than alternative methods that require multiple solutions of the full transient problem. Note that the same simulator we use for the forward problem is used to obtain the steady-state solutions.

Verification of Sensitivities. The sensitivity expressions for both S'_w and S'_g consist of a fractional flow and a divergence of flux term. For incompressible flow, the divergence of flux term vanishes. For compressible flow, the divergence term tends to dominate at early times and the fractional flow term dominates when the flow is fully developed. **Fig. 6** shows a comparison of the gas/oil ratio sensitivity and the divergence of flux at three different stages for a synthetic quarter-five spot model. From the top to the bottom of **Fig. 6**, it is obvious that we transition from a divergence of flux dominated sensitivity to flow dominated sensitivity. This is highlighted by the loss of similarity between the divergence of flux and the GOR sensitivity with a concurrent increase in the alignment of the sensitivities to the trajectory of the streamlines along which fluid transport is calculated.

Transforming the Observed GOR and WCT for History Matching. We described earlier the travel-time sensitivity of the composite quantities, S'_w and S'_g for three-phase flow. In order to compute the travel-time misfit between the observed and simulated response, it is necessary to transform the observed GOR and WCT data to these composite saturation quantities. In the discussion on sensitivities, we stated that given a pair of GOR and WCT observation, there is a corresponding characteristic pair of gas and water saturation. Let us now look at this in more detail starting with the following relations,

$$GOR = \frac{Q_g}{Q_o} = \frac{Q_{g,free} + R_s Q_o}{Q_o} = \frac{Q_{g,free}}{Q_o} + R_s = \frac{k_{rg}\mu_o B_o}{k_{ro}\mu_g B_g} + R_s \quad \text{..... (24)}$$

and

$$WCT = \frac{Q_g}{Q_o + Q_w} = \frac{1}{1 + \frac{Q_o}{Q_w}} = \frac{1}{1 + \frac{k_{ro}\mu_o B_w}{k_{rw}\mu_w B_o}} \quad \text{..... (25)}$$

These equations show that with the pair of observation data and a flowing bottom-hole pressure, we can iteratively solve for the corresponding pair of gas and water saturations given a PVT data set and a set of relative permeability curves. Once we obtain the unique saturation pair, we then

transform each observed pair of water-cut and GOR data to S'_w and S'_g respectively. Similarly, for the simulated response, we compute the transformed quantities. It is these transformed quantities (S'_w, and S'_g vs. time) that we use to compute the travel time misfit between observed and simulated response as illustrated in **Fig. 2**. A match on both quantities ensures a match on the observed gas/oil ratio and water-cut as shown in **Figs. 2,** and **4.**

To illustrate the significance of the data transformation, **Fig. 7** shows a comparison of the observed gas/oil ratio and its transformed equivalent. Also shown is the misfit computation using GTTI on both data. It is obvious that the transformed data gives a profile more amenable to shift time computation. In this particular instance, computed optimal shift with the observed data is 12 days. This is erroneous as it suggests a close agreement between the observed and simulated profiles. The optimal shift using the transformed data however is about 200 days, a more realistic estimate.

In our proposed approach, it is required that we have measurements of BHP at each observation. It should be noted that in the absence of the pressure data, we can not uniquely define S'_w and S'_g and also there is no guarantee that the reservoir energy has been adequately reproduced, thus limiting the value of the calibrated model. This further emphasizes the importance of pressure data in model calibration during compressible flow. For the common case of infrequent pressure data points, we recommend an initial match on the available pressure data alone. With the resulting pressure profile, production data can be transformed to the composite saturation quantities and a simultaneous match on the water-cut, gas/oil ratio, and BHP can then be done in the manner described here.

Misfit function and minimization

Reconciling geologic models to dynamic data typically involve the solution of an inverse problem. Various approaches for such data integration have been proposed in the literature and they can be broadly classified as either deterministic or Bayesian.[14] While our method can be formulated either way, we discuss the deterministic approach here. The basic underlying principles behind the history matching algorithm are as follows.

- Match the field production history within a specified tolerance. This is accomplished by minimizing the travel time misfit for the transformed saturation quantities.
- Preserve geologic realism by keeping changes to the prior geologic model minimal, if possible. This is because the prior model already incorporates static data (well and seismic data) and available geologic information.
- Allow for smooth and large scale changes because production data has low resolution and cannot be used to infer small scale variations in reservoir properties.

Mathematically, these objectives lead to the minimization of a penalized misfit function. Additional constraints are imposed to ensure "plausibility" and stability of the solution.[1, 10] These include a ‘norm’ constraint that minimizes the deviation from a prior geologic model and a ‘roughness’ constraint that allows for large-scale changes only consistent with the low resolution of the production data both of which satisfy the second and third objectives above.[14] The penalized misfit function thus consists of the following terms:

$$\left\|\Delta \mathbf{t} - \mathbf{S}\delta\mathbf{R}\right\|_2 + \gamma_1\left\|\delta\mathbf{R}\right\|_2 + \gamma_2\left\|\mathbf{L}\delta\mathbf{R}\right\|_2 \quad \text{..... (26)}$$

In **Eq.26**, $\Delta\mathbf{t}$ represents the stacked vector of generalized travel-time shift at the wells for both saturation quantities (S'_w, and S'_g), and zero frequency pressure misfit. $\mathbf{S}$ is the stacked matrix of the sensitivity of generalized travel-time with respect to the reservoir parameter for both saturation quantities, and the zero frequency pressure sensitivity to reservoir parameters., $\mathbf{L}$ is a roughness operator given by the second spatial derivative and $\delta\mathbf{R}$ is a vector representing the change in reservoir parameters during iterative model update. The weights γ_1 and γ_2 determine the relative strengths of the norm and smoothness constraint and guidelines exist in the literature for their selection. An iterative sparse matrix solver, LSQR[12], is used for solving the augmented linear system efficiently.

Applications

A Field-Scale Synthetic Case: The SPE Example

Our first field-scale example is the ninth SPE comparative study. The reservoir (**Fig. 8**) is represented by a 24×25×15 mesh with rectangular coordinates. The dimensions of the grid blocks are 300 feet in both the X- and Y- directions. Cell (1, 1, 1) is at a depth of 9000 feet sub sea at the center of the cell top. The remaining cells dip in the X-direction at an angle of 10 degrees. Values of porosity and thickness can be found in the paper by Killough.[15] The total thickness from Layers 1 to 13 is 209 feet (16 feet per layer in average), and Layers 14 and 15 have thickness of 50 and 100 feet respectively.

Fluid properties and relative permeability data are the same as provided for the comparative study. For our purposes, we have used the original permeability field of the comparative study as a true or reference model to generate production history from flow simulation.

A total of 1 water injector (I1) and 25 producers (PROD1 to PROD25) were included in the simulation model. The injector was completed from layers 1 through 11. All producers except producers 8, 16, 22, and 25 are completed in layers 1 to 13. These producers are completed in layers 1 to 5 in order to avoid completion in the water leg.

In order to generate a starting permeability field for the calibration exercise, we have geostatistically created a permeability realization from the original permeability field using the well data as control points. With this starting model, we follow through the procedure of data transformation, sensitivity calculation and minimization to reconstruct the original permeability field provided for the comparative study. In seven iterations of the joint inversion, all the wells showed good matches on the transformed composite saturation quantities and thus, the water-cut and gas/oil ratio. **Fig. 9** shows the match obtained on a few of the wells. Again, the result emphasizes that a simultaneous match on the transformed data ensures a match on the measured quantities (water-cut and gas/oil ratio). On a global scale, comparing the histogram of the updated permeability field to the reference (**Fig. 10**), a visual inspection indicates that we have a better representation of the permeability distribution (Log Normal) after the inversion

Since in this case, we have access to the true permeability field, we carry out more detailed analyses on the results of the inversion. We compared the changes made to the initial permeability field to those needed to be made for complete reconstruction of the reference permeability field. **Fig. 11** is a random selection of layers showing a comparison of the changes made by the inversion algorithm to those needed. It is clear that we have captured, directionally, the permeability change required in most cases. The changes are guided mostly by the streamline trajectory along which the sensitivity calculations are done. In essence, in areas of low cluster of streamlines over the duration of the simulation, changes made may be inaccurate. This partly

explains the inconsistent changes made in some of the layers. That we lack resolution on a layer basis as would otherwise be provided by spinner data for instance, could be another reason for the few inconsistent changes made. As stated earlier, while we adjust the permeability to match the production data, we impose a 'norm' constraint to preserve the prior geologic model. **Fig. 12** shows the permeability distribution on a layer before and after the inversion. While the changes are obvious on this layer, we still see the imprint of the prior model. Overall, the match is satisfactory and the prior model is preserved.

A West African Field Case

The field case is a highly faulted, west-African reservoir from which production started early in 1971 with an underlying aquifer providing some pressure support. The reservoir model consists of twelve layers with each layer sub divided into a 182 by 51 grid of cells (**Fig. 13**). Fluid property in the reservoir is modeled by five sets of PVT data corresponding to the different identified equilibrium regions. The rock-fluid property is modeled by a normalized relative permeability curve with the end-points and critical saturations of each cell specified. The reservoir is produced under depletion with three producers (Well 17D, Well 21, and Well 41) downthrow of the major fault. Well 17D is completed in layers 6 through 8 and has over thirty years of production history without significant water production. Well 21, also completed in the same interval has observation limited to the early years of production. Well 41 is a more recent well completed in layers 3, 6, and 7. Of the three, Well 41 is the only well that has substantial water production. While there is sufficient pressure information on well 17D, the only pressure information available is a static BHP survey done in wells 17D and 21 and a RFT test done in well 41.

In calibrating the reservoir model we first match the observed pressures using the low-frequency asymptotic approach by matching the zero-frequency component of the Fourier transformed data.[11] With the resulting pressure match (**Fig. 14**), there was sufficient information for transforming the production data to saturation components. Next, we proceed with the iterative simultaneous integration of dynamic data as described above. **Fig. 15** shows the misfit reduction achieved for the saturation match. In 16 iterations, both the amplitude and travel time misfit have been reduced to twenty five percent of their initial values. While 16 iterations seem like many compared to our previous work using streamline-derived sensitivities, this is partly because of the complexity of the problem and the fact that production is under primary recovery. **Fig. 16** shows the match of the observed production data. Overall, we have acceptable matches on the observed data. With limited production from Well 21, model calibration was done using mostly data from the other wells. While production from this well was limited, the pressure observation from the well was useful information for our purposes. Changes made during the inversion are limited to those regions as dictated by the sensitivities computed along the streamline trajectories. An illustration of this is seen in **Fig. 17** through the pre and post inversion permeability histograms and statistics. Much of the prior statistics are preserved after the inversion. Furthermore, **Fig.18** highlights regions in the model where changes were made to the permeability field on a layer by layer basis. It is clear that the prior model is for the most part retained.

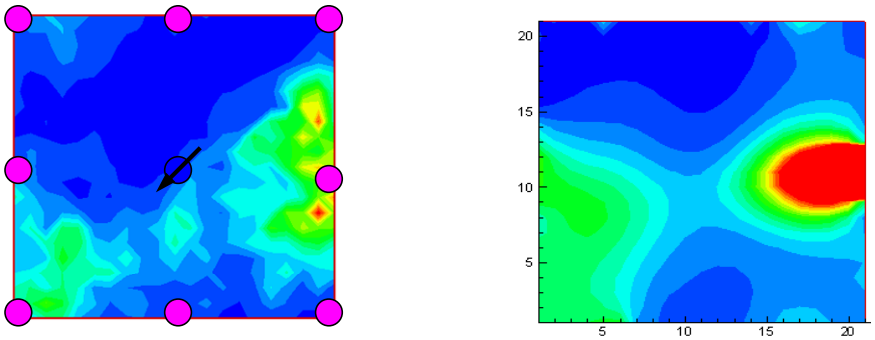

(a). Reference Permeability Field (b). Reconstructed Permeability Field

Fig. 1 Synthetic case: Comparison of reference and reconstructed Permeability fields

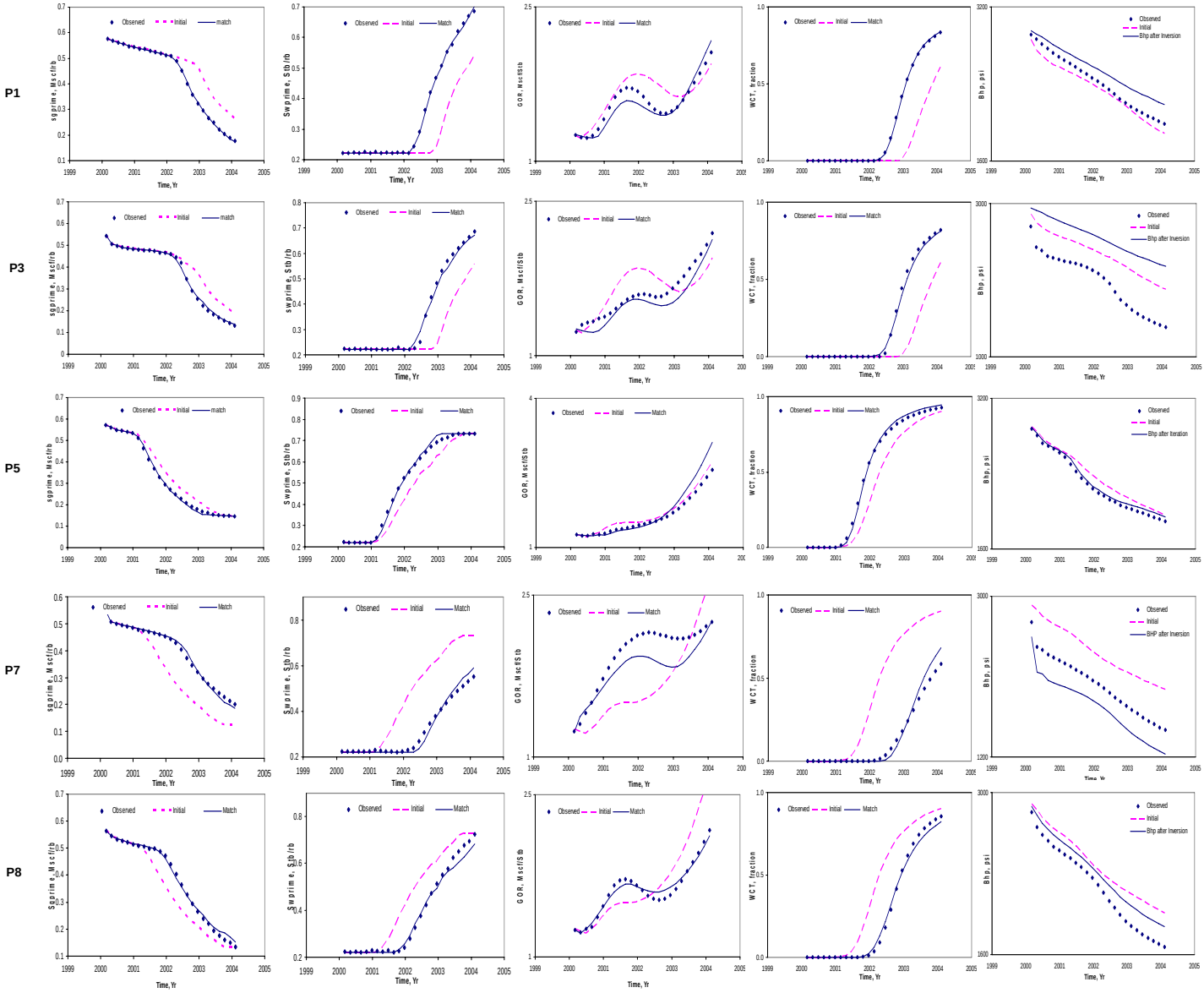

(a). Normalized GOR (b).Normalized WCT (c). Gas-Oil Rati (d) Water-cut (e). BHP after Inversion

Fig. 2 History matching 3-phase flow for a Synthetic nine-spot heterogeneous case: Match and BHP Comparison

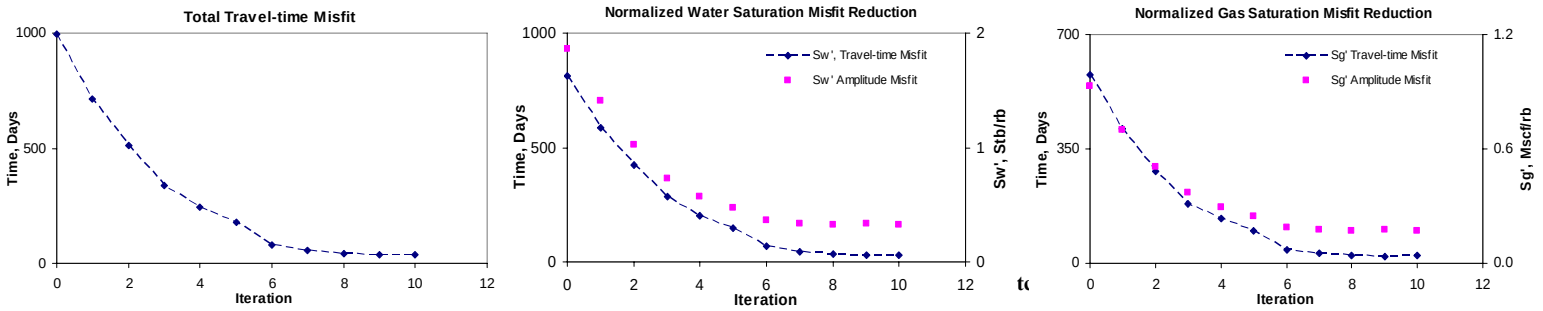

Fig. 3 Nine Spot Synthetic Case: Rapid Convergence of GTTI on transformed composite saturation quantities

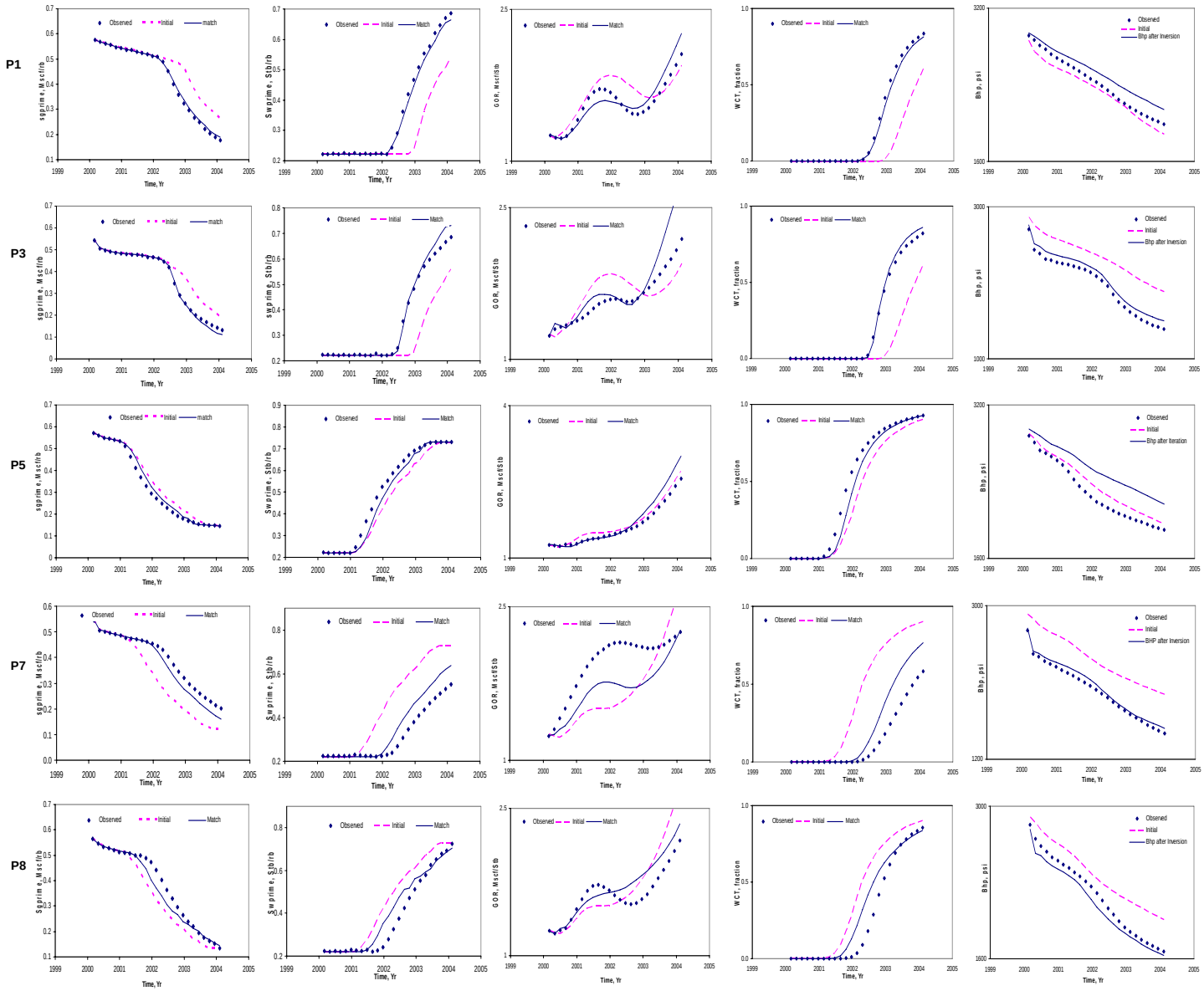

(a). Normalized GOR (b). Normalized WCT (c). Gas-Oil Ratio (d) Water-cut (e). BHP Inversion

Fig. 4 History matching 3-phase flow for a Synthetic nine-spot heterogeneous case: Joint Inversion of WCT, GOR, and BHP

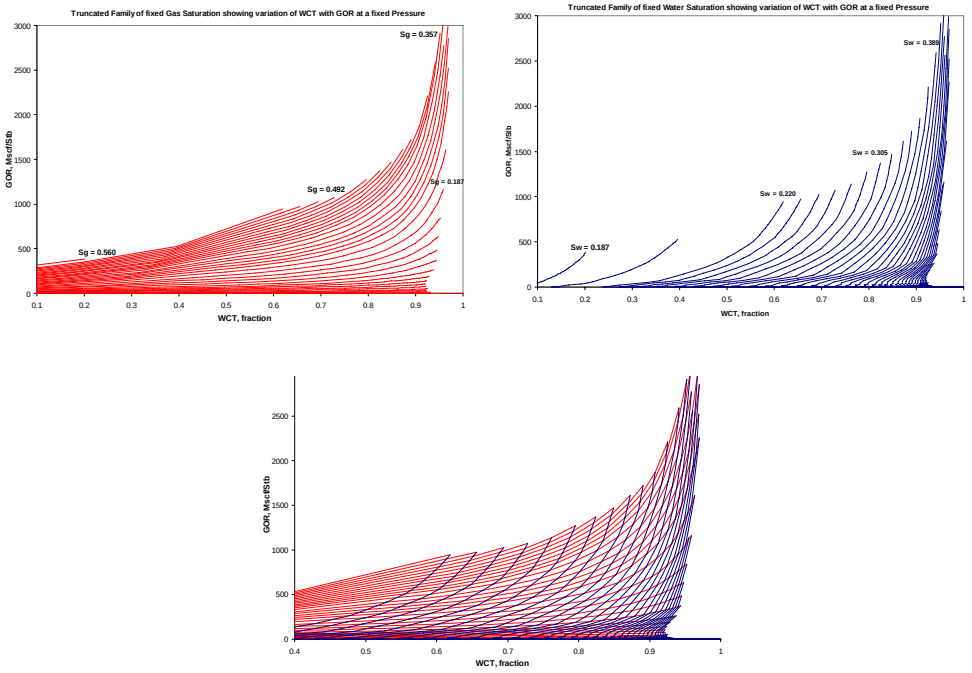

Fig. 5 Plots showing truncated families of fixed water and gas saturation showing the unique correspondence between a pair of GOR / WCT data and a pair of Sg/Sw using PVT and SCAL data from the ninth SPE comparative study[15]

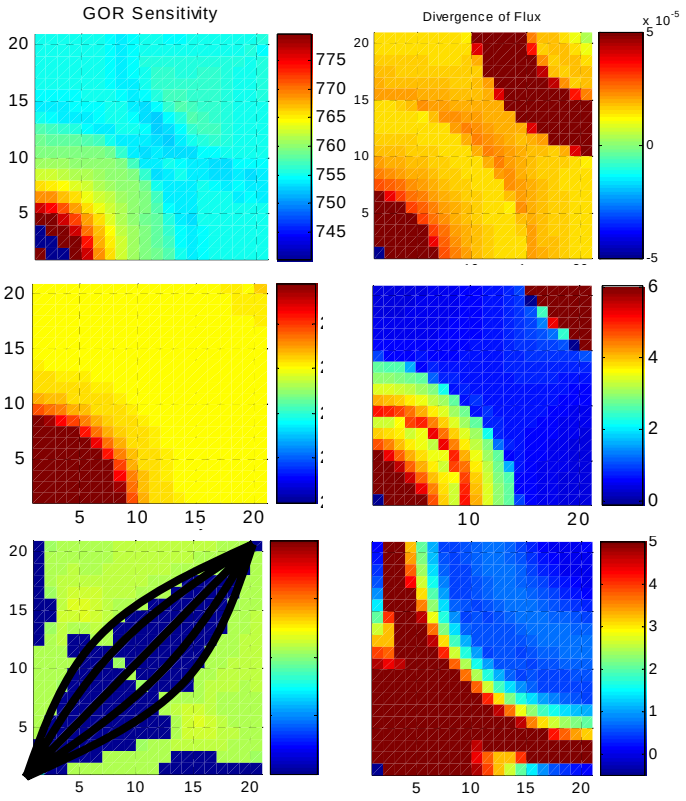

(a). GOR Sensitivity **(b). Divergence of Flux**

Fig. 6 Verification of Analytical Sensitivities: The two components of the sensitivity dominate at different times.

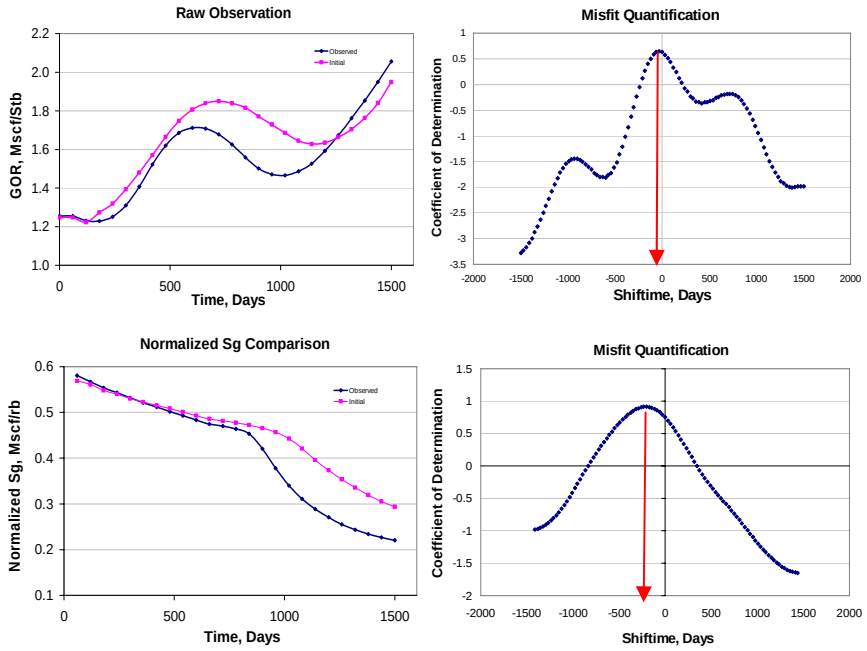

(a) Observed (Top) and Transformed (Bottom) data (b) Misfit quantification on observed (top) and Transformed (Bottom) data

Fig. 7 Transformation of observed data (WCT and GOR) to composite saturation quantities and misfit quantification

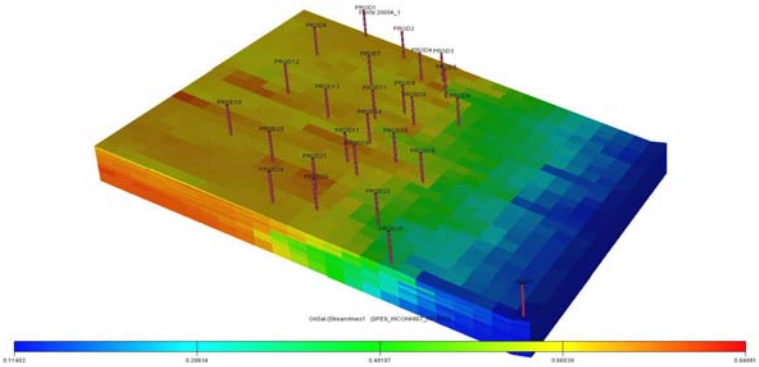

Fig. 8. Field-Scale Synthetic case: Modified SPE9 Model (25 Producers and 1 injector)

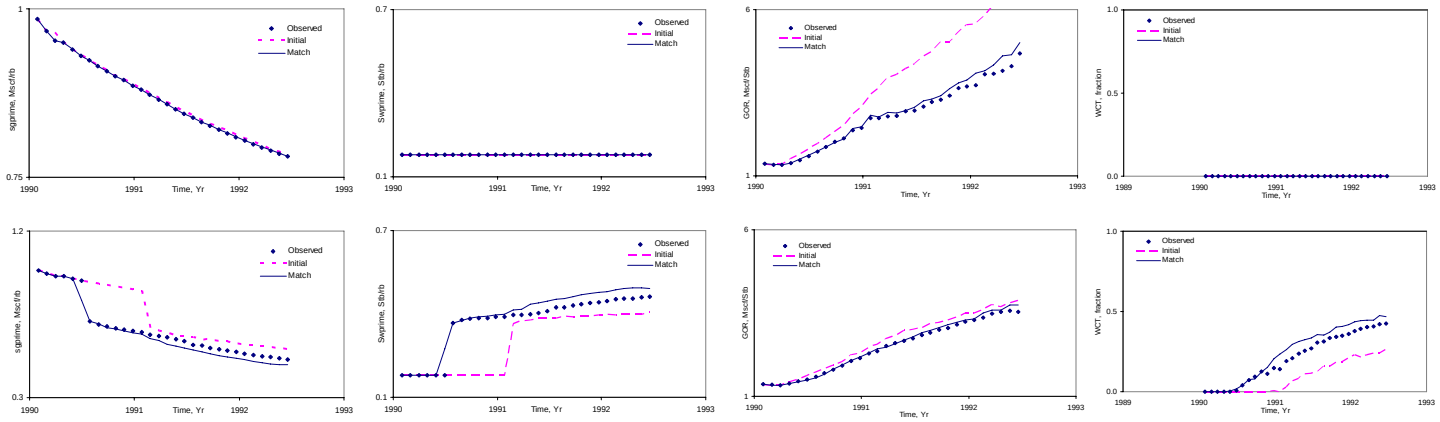

(a). Normalized GOR (b). Normalized WCT (c). Gas-Oil Ratio (d) Water-cut

Fig. 9 History matching 3-phase flow for a 3-D Synthetic case

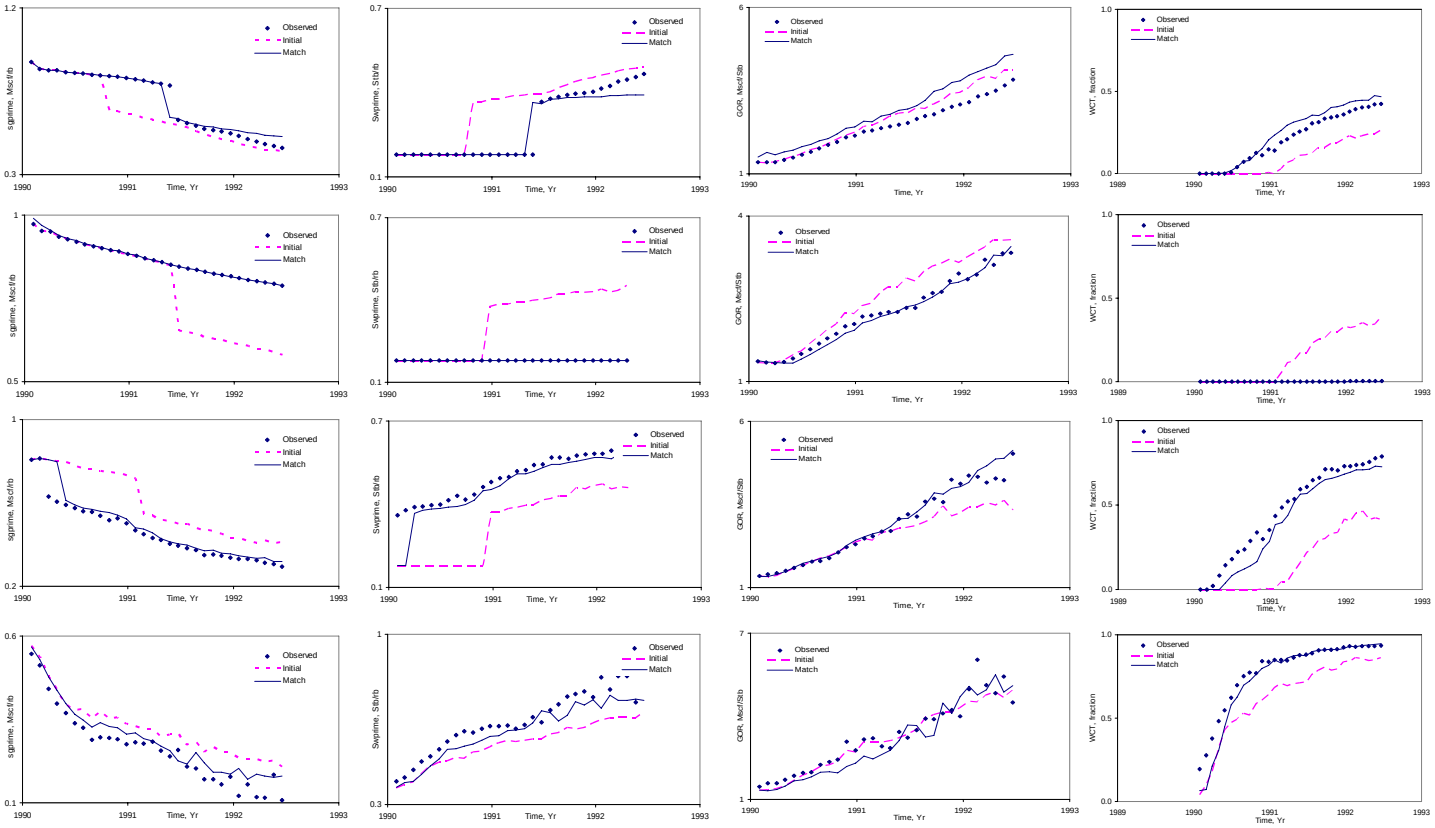

(a). Normalized GOR **(b). Normalized WCT** **(c). Gas-Oil Ratio** **(d) Water-cut**

Fig. 9 (Contd.) History matching 3-phase flow for a 3-D Synthetic case

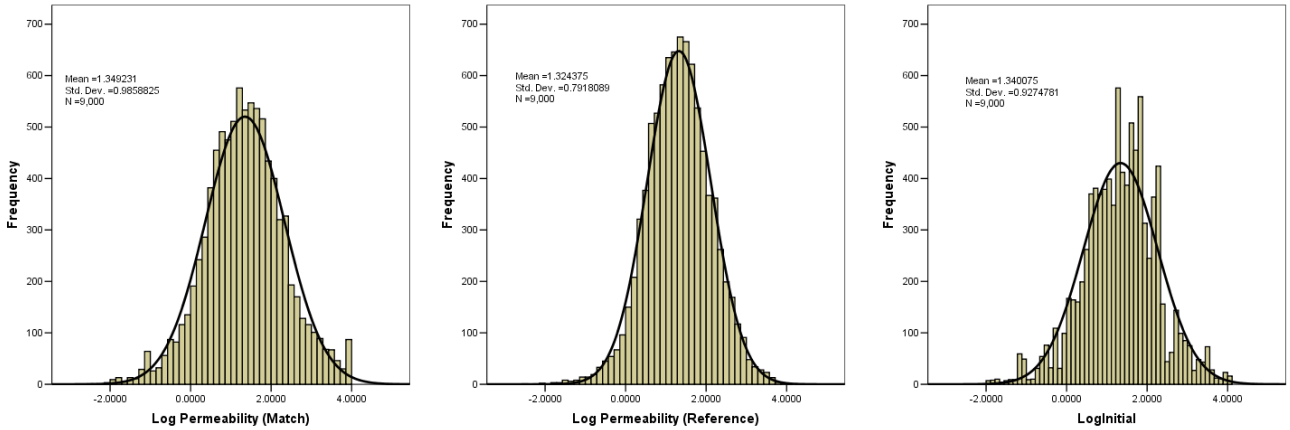

(a). After Inversion **(b) Reference** **(c) Initial**

Fig. 10 Histogram and statistics of permeability field

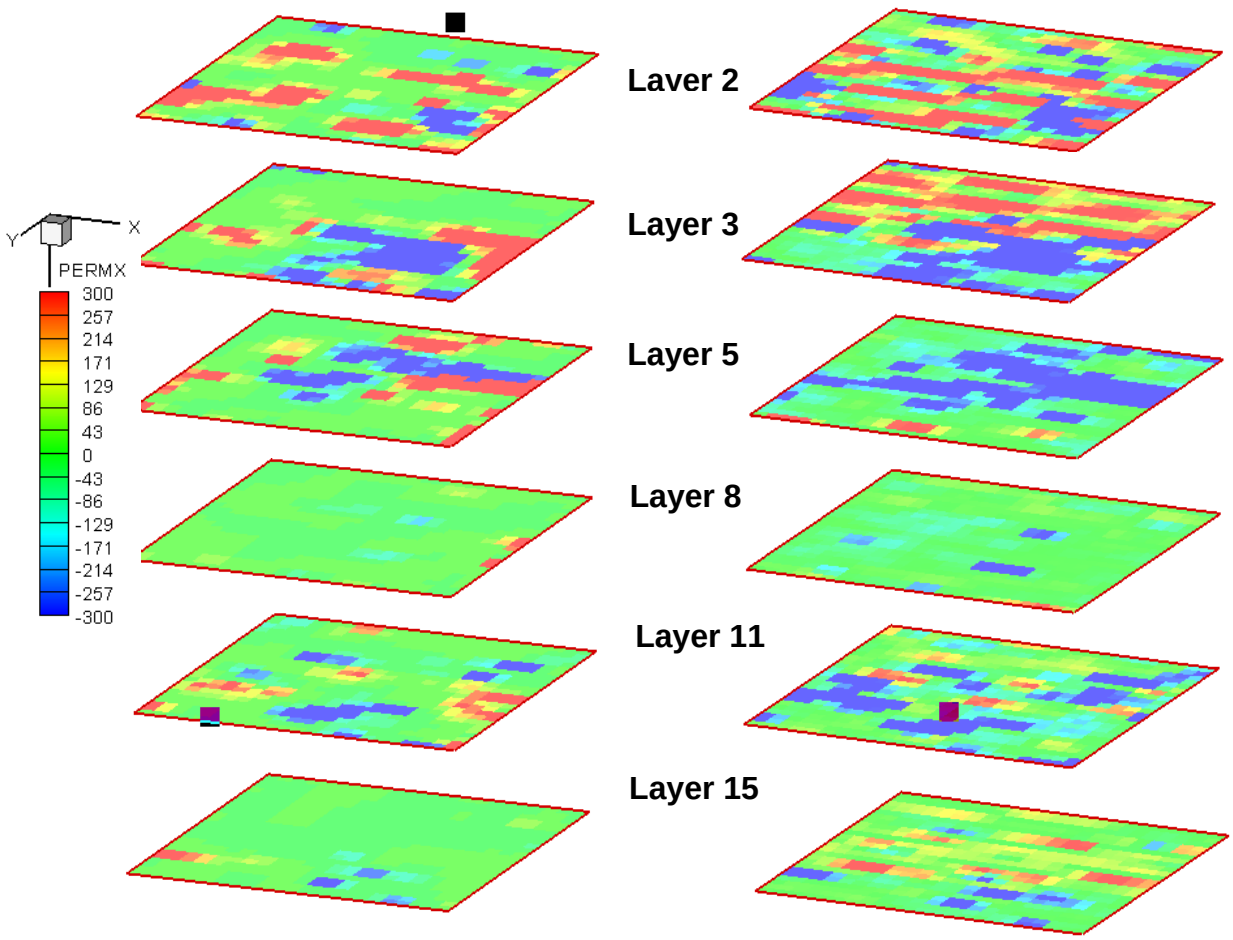

(a). Permeability changes made (b) Permeability changes needed

Fig. 11 Layer comparison of changes made and changes required

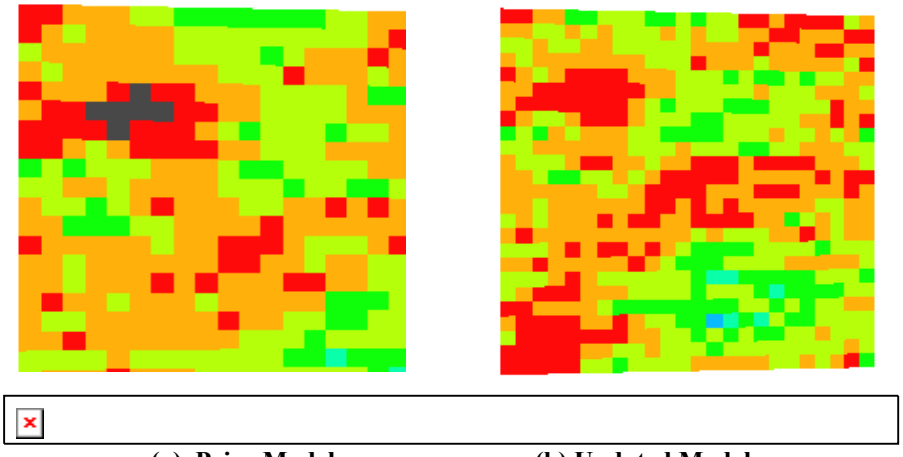

(a). Prior Model (b) Updated Model

Fig. 12 Preservation of prior Model after inversion

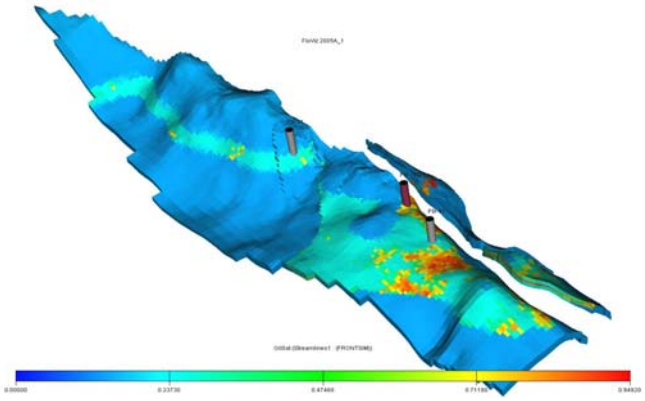

Fig. 13 Reservoir Model

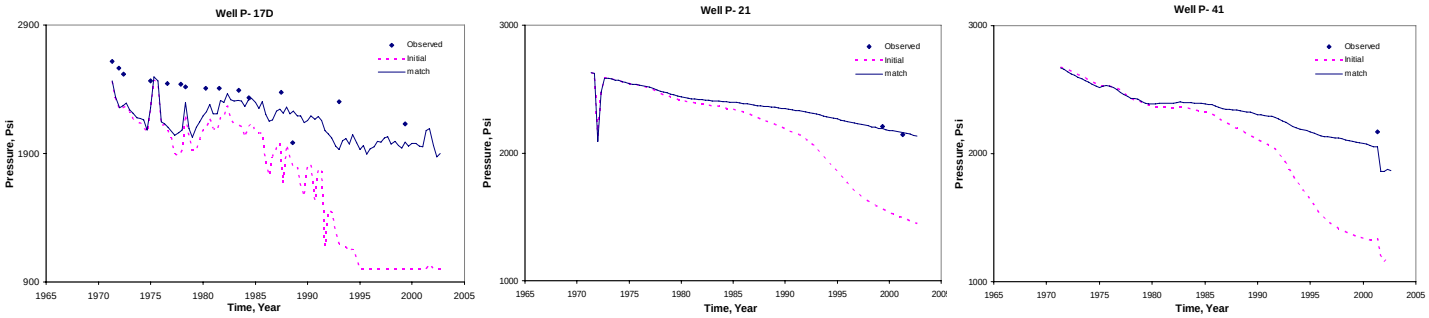

Fig. 14 History matching 3-phase flow for a Field case: Initial match on Pressure Observation

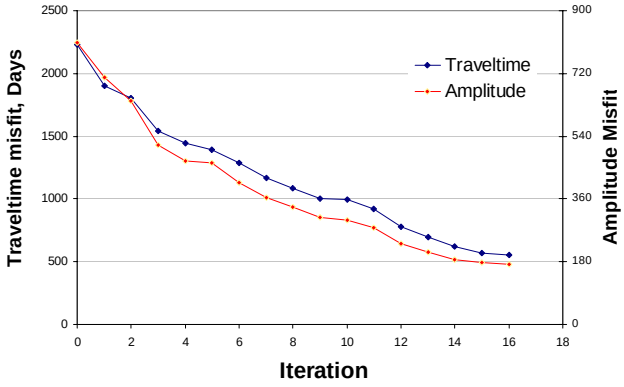

Fig. 15 History matching 3-phase flow for a Field case: Misfit reduction

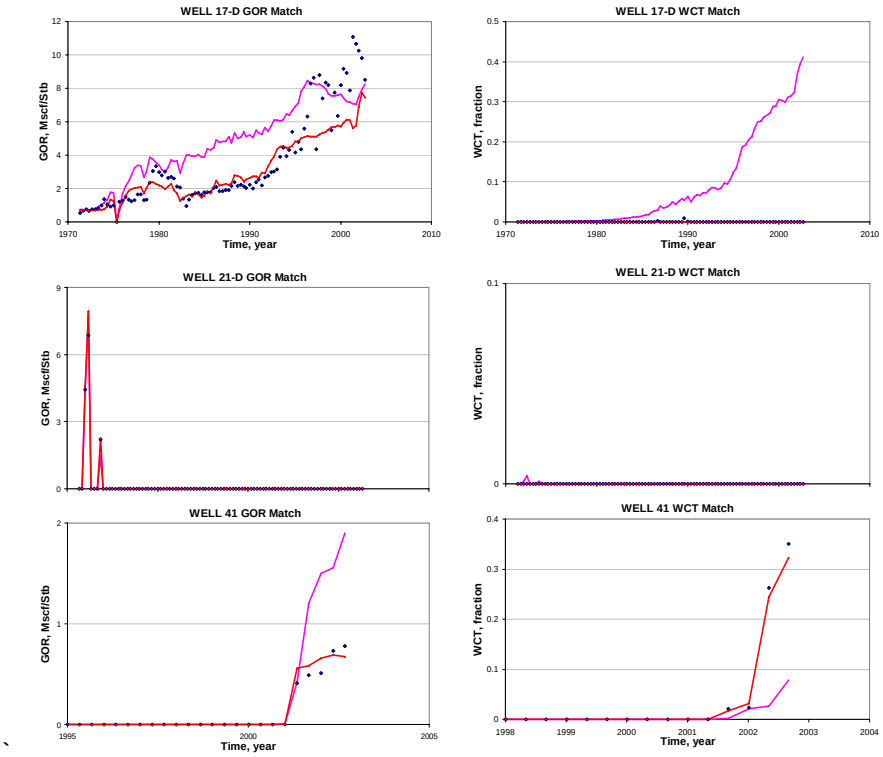

Fig. 16 History matching 3-phase flow for a Field case: Match on GOR (Left), and WCT (Right) after inversion

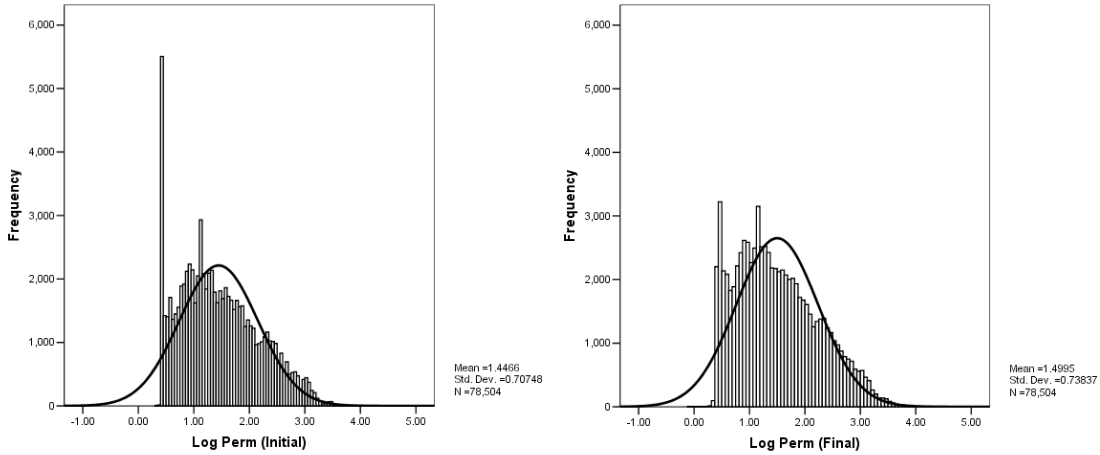

Fig. 17 Histogram and statistics of Permeability field before (Left) and after (Right) inversion

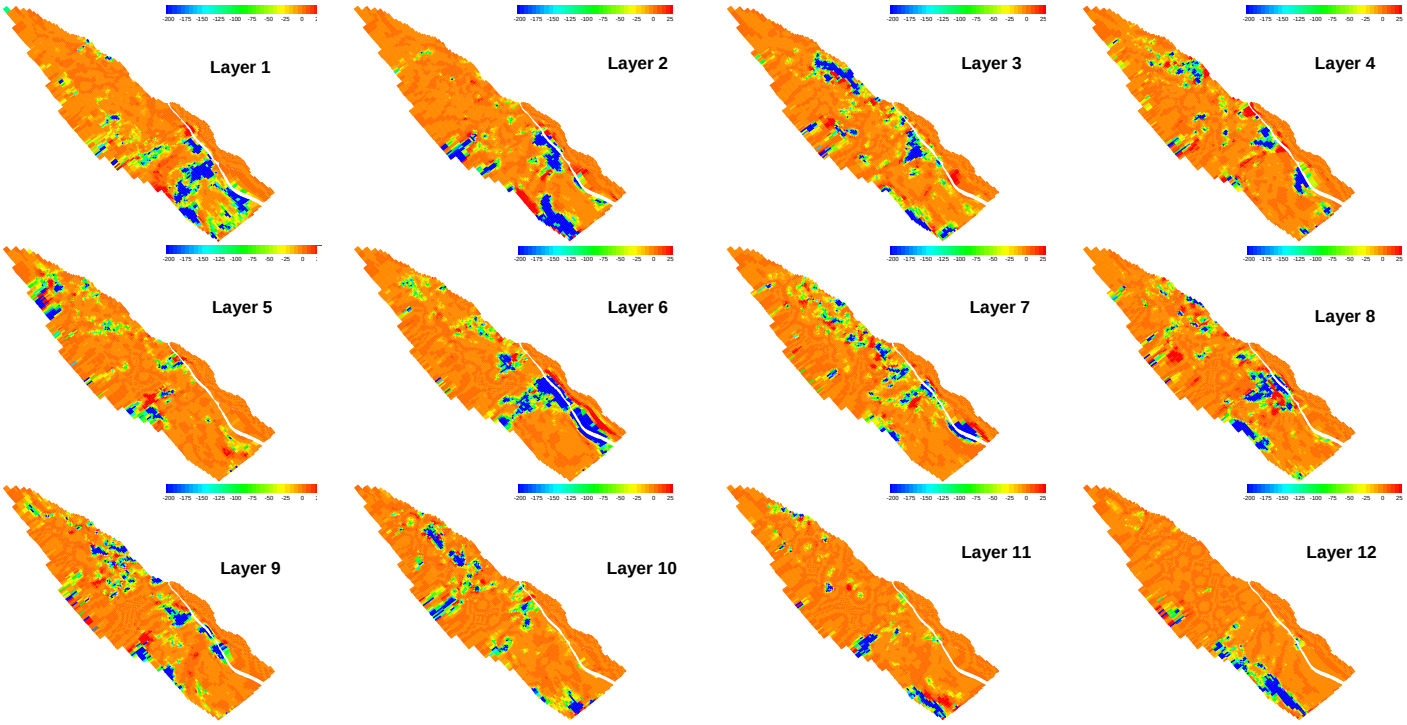

Fig. 18 Field Case: Plot showing regions where changes have been made to the prior model for the History Match

RESULTS AND DISCUSSION: PART II

Reservoir Model Updating and Uncertainty Assessment Using Ensemble Kalman Filter with Sensitivity-based Covariance Localization

In recent years, there has been a paradigm shift from attempting to 'history match' a single reservoir model to generating a suite of realizations consistent with all dynamic data and prior geologic information. Predicting future reservoir performance with these multiple realizations would provide for a measure of uncertainty in model forecasts, leading to better reservoir development and management strategies. This effort has been aided by the development of robust and efficient algorithms for automatic and assisted history matching,[1-3] and availability of greater computational power. The Ensemble Kalman Filter (EnKF) is one such promising technique for generating a suite of plausible reservoir models.[4-10] The EnKF samples from multi-dimensional probability density functions (pdf) that are consistent with our prior knowledge of the model parameters. These samples or realizations help specify covariances between model parameters and cross-covariances that relate measurements and model parameters. Instead of computing gradients as in variational methods, these covariances and cross-covariances are utilized to update the models.

The increased deployment of permanent downhole sensors and intelligent well systems that provide a continuous stream of information has made the EnKF an appealing method for sequential model updating.[4-10] The capability to maintain 'live models' combined with the ability to assimilate diverse data types and the ease of implementation have resulted in increased research effort and interest in the EnKF.

In spite of its appeal, there are still outstanding challenges pertaining to the use of this technique. For practical field applications, the EnKF would be viable if the ensemble size could be kept small for computational efficiency. Experience has shown that small ensemble sizes also lead to erroneous cross-covariance estimation, particularly for grid points widely separated from the location of the observed data. This degrades the EnKF forecast as more data is assimilated. One important aspect in history matching is maintaining geologic continuity, that is, the final model should reproduce the large-scale flow paths and barriers within the reservoir. The EnKF tends to transform multi-modal permeability histograms to a more normal or Gaussian distribution over a sequence of many updates.[10] Because of its maximum entropy characteristics, the Gaussian fields cannot reproduce the continuity of the extreme values, that is, the high permeability channels and low permeability barriers that significantly impact fluid flow in the reservoir. Previous literature in EnKF has also reported parameter overshoots/undershoots resulting in localized patches of low and high permeabilities that can lead to loss of geologic realism.[4-6] The use of these 'history matched' suite of models for future forecasts or uncertainty analysis can cause erroneous interpretation and sub-optimal field development strategies.

A larger ensemble size will help reduce many of the above-mentioned problems. In previous applications of the EnKF in reservoir characterization, an ensemble size of 50-100 models was deemed sufficient. However, this is likely to be problem specific. Increasing the ensemble size to adequately capture the cross-covariance between the model parameters and measurements is computationally demanding, particularly for large-scale field applications.

In this work, we describe an approach to mitigate some of the difficulties in the application of the EnKF for reservoir history matching. The primary appeal of our proposed approach is that

the updated model realizations tend to retain the initial geological features. Over a sequence of many EnKF updates, our approach maintains the shape of the initial permeability histogram by targeting and limiting changes to the prior model. This is accomplished by identifying 'regions of influence' for individual data points using parameter sensitivities. Our approach also controls the parameter overshooting reported in earlier implementations of the EnKF. Most importantly, all these are accomplished using a relatively small ensemble size.

The essence of our approach is to utilize streamline-based sensitivities to modify or condition the cross covariance between production data and the model parameters. This does not entail an increased computational effort because the streamline-derived sensitivities are obtained analytically during the forward run of the simulator.[1, 11-14] Our approach is equally applicable to both streamline and finite-difference simulators. For finite-difference simulators, the streamlines can be easily generated based on the velocity field.[15] The ensemble based cross-covariance estimates are multiplied element by element with a weighting function computed from these analytic sensitivities. It has been shown that such 'covariance localization' is equivalent to using a larger ensemble of realizations in reducing errors in the cross-covariance estimates.[16]

The outline of our report is as follows. First, we briefly review the major steps in the EnKF and show how errors in the cross-covariance calculations affect the analysis. We also show how these errors can be reduced with an increased ensemble size. This is followed by a brief discussion of the streamline-based sensitivity computations and their use to condition the cross-covariance matrix in EnKF. We then illustrate the benefits of covariance localization using a synthetic example and examining the eigenvalue spectrum of the parameter covariance matrix. Finally, we demonstrate the power and practical utility of the approach using the benchmark SPE9 example involving three-phase flow and a field example from West Texas.

Basic Steps of the Approach

Sensitivities between production data and model parameters quantify and relate changes in production response at a well because of small changes in reservoir parameters. Thus, sensitivities identify regions in the reservoir where changes in the parameters will have an influence on the model prediction. Several approaches can be used to compute sensitivity coefficients of model parameters. In particular, streamline models allow us to analytically derive the relationship between perturbations in model parameters and changes in well responses, for example, water-cut and GOR.[1,11-14] Most importantly, these streamline-based sensitivities can be computed simultaneously with the forward simulation resulting in significant computational efficiency.

In EnKF, the cross-covariances computed from an ensemble of models are used to update the models at a given time. The cross-covariance calculations relate reservoir parameters to dynamic responses of the reservoir. In our proposed approach, these cross-covariances are weighted with a function related to the streamline-derived sensitivities. Our objective here is to eliminate spuriously large terms in the cross-covariance matrix resulting from a limited size ensemble. At each update step, the streamline derived analytic sensitivities are utilized to condition the cross-covariance calculations. Other applications of cross-covariance conditioning have been reported in atmospheric data assimilation literature where a distance-dependent correlation function is utilized.[16-17] The idea behind these previous approaches was to improve the EnKF analysis by excluding observations greatly removed from the grid point being analyzed by the use of a cut off radius.

The advantage of the streamline-based covariance-localization is its close link to the underlying physics of flow compared to a simple distance-dependent covariance function as used in the past.[16] For fluid flow in highly heterogeneous media, the presence of flow channels can cause production response to be affected by permeabilities at large distances from the well. A distance dependent correlation function will artificially dampen the influence of these permeabilities. On the other hand, the streamline-derived sensitivities rigorously define the region of influence of the production data. Furthermore, it also quantifies the relative impact of grid block parameters on the production response. This makes the sensitivity-based covariance localization particularly attractive. The major steps in our proposed approach are outlined below.

- **Ensemble Forecast Step**. Using our prior knowledge of geology and static data, we generate a suite of reservoir models. We compute the dynamic response from each of these models up to the next available observation time using either a streamline or a finite-difference simulator. Simultaneously, we obtain the streamline-derived analytic sensitivities for the grid block parameters. For finite-difference simulators, these require an additional step of generating the streamlines and computing the time of flight[15].
- **Covariance Localization.** For the well observation and the time of interest, we threshold the sensitivities using a sufficiently small cut-off to identify a 'region of influence' for the observation. We then stack the region of influence from all ensemble members to define a 'common region of influence'. In EnKF, we compute the cross-covariance with respect to the grid blocks within this region only. The cross covariance matrix is then weighted term-by-term using a covariance filter function derived from the sensitivities. This filter function has a maximum value of 1.0 and progressively decreases as the magnitude of the sensitivities decreases. It is simply a normalization of the absolute values of the sensitivities computed from all ensemble members.
- **The Ensemble Update.** The cross-covariances computed in the previous steps are used to first estimate the 'Kalman Gain' which relates changes in model parameters to the data misfit (**Eq. 6** discussed later). Finally, the ensemble members are updated using the 'Kalman Update' equation (**Eq. 4** given later). The procedure is repeated until all the production data are assimilated.

A step-wise outline for our proposed approach is given in the flow chart in **Fig. 1.** It only requires an additional step of sensitivity computation and covariance localization compared to a standard EnKF implementation. Because streamline-based sensitivities can be obtained easily during forward flow simulation, the extra computational overhead is minimal.

The Benefits of Covariance Localization. In a previous paper, we illustrated the benefits of covariance localization using information from the streamline trajectories.[10] The standard EnKF approach developed by Evensen[18, 19] and later introduced to petroleum engineering literature by Nævdal *et al*[6] was shown to be incapable of reproducing the bimodal nature of the permeability histogram after a sequence of updates. The bimodal permeability histogram was transformed into a Gaussian distribution that could not reproduce the connectivities of low and high permeabilities. Covariance localization, on the other hand, helped maintain the bimodal nature of the permeability histogram and was capable of retaining many of the geologic features present in the initial realizations.

In this section, we illustrate the necessity and implications of our proposed sensitivity-based covariance localization in EnKF using a 2D synthetic example. Our goal is to update permeability distribution using waterflood response in a five-spot pattern. We use the standard EnKF with flow simulation on a 41x41 grid. Three different ensemble sizes for permeability distribution were used: 40, 100 and 400. The reference permeability field is shown in **Fig. 2.** Also superimposed are the streamline trajectories and time of flight. **Fig. 3** shows the streamline trajectories and the normalized sensitivities to water-cut for two producing wells for a particular realization for a specific time.

We can realize the significance of the covariance localization by examining the eigenvalue spectrum of the parameter covariance matrix.[16] For this purpose, we compare the results from the standard EnKF with our proposed sensitivity-based covariance localization, referred to as the 'conditioned EnKF'. **Fig. 4** shows the eigenvalue spectrum for the permeability covariance matrix after a sequence of EnKF updates for three different ensemble sizes. Assuming that the 400-member ensemble specifies a realistic eigenvalue spectrum, we can see that using the conditioned EnKF tends to retain the character of the 'true' spectrum. However, without covariance localization, the standard EnKF leads to a steep drop in the spectrum, which means that there is insufficient projection of the variance in the direction of the trailing eigenvectors. The low energy present in these directions results in a smaller effective ensemble size, reducing the search space of the model parameters and resulting in a poorer estimation of the covariances. Therefore, without localization the covariance structure is easily degraded, leading to poor parameter estimates and potentially filter divergence.

Fig. 5 shows the updated permeability distribution after assimilating water-cut data using EnKF with and without covariance localization. Clearly, without covariance localization, the changes to the permeability field appear to be more random and the updated field shows significant deviations from the initial permeability distribution (**Fig. 5b**). However, using the conditioned EnKF, we are able to preserve most of the features of the prior model. The changes are hard to discern because they are specifically targeted and kept minimal (**Fig. 5c)**. This allows us to preserve geologic features during history matching. To illustrate further the implications of the covariance localization, in **Figs. 6a** and **6b** we have shown the cross-covariance between the water-cut for one of the wells and the grid block permeabilities for a particular assimilation time. We can see that the standard EnKF shows spuriously large cross-covariance for distant grid blocks and these are effectively damped through the localization.

Implementation of the EnKF and Calculation of Streamline-based Sensitivities

This section briefly discusses the EnKF and the implementation of our proposed enhancements using the streamline-derived sensitivities.

The Reservoir State Vector. In EnKF, the true state vector, $\boldsymbol{y_k}$, that we are trying to estimate at time k, could include static variables $\mathbf{m}_k^s$ (e.g. permeability, porosity), dynamic variables $\mathbf{m}_k^d$ (e.g. pressure, phase saturation), the production data $\mathbf{d_k}$ (e.g. bottom-hole pressure, water-cut and gas-oil ratio at the wells) and other observed responses, for example, 4-D seismic surveys. Static information from well logs, core data and seismic surveys along with geologic information helps us build a set of realizations based on the prior knowledge. Equivalently, this can be interpreted as random samples from the prior probability distribution function (pdf) of these parameters. A large enough set of realizations would capture the dispersion in these parameters and the

covariance matrix of these parameters reflects the variability around an expected value. The EnKF uses this ensemble of realizations to compute a mean and a covariance of the model parameters.

The ensemble of state vectors is represented by **Eq. 1** below.

$$\boldsymbol{\Psi}_k^p = \left\{ \mathbf{y}_{k,1}^p \quad \mathbf{y}_{k,2}^p \quad \cdots \quad \mathbf{y}_{k,N_e}^p \right\} \quad \text{..... (1)}$$

where the state vector $\mathbf{y}_k^p$ for each realization at time *k* is defined by **Eq. 2**.

$$\mathbf{y}_k^p = \begin{Bmatrix} \mathbf{m}_k^s \\ \mathbf{m}_k^d \\ \mathbf{d}_k \end{Bmatrix} \text{.....(2)}$$

The superscript *p* denotes prior, *s* stands for static and, *d* stands for dynamic. Also, N_e represents the number of ensemble members.

The EnKF Forecast and Update. The EnKF uses a forecast step to evolve the state vector using the dynamics of the physical phenomena under study. In reservoir simulation, this involves running the numerical simulator up to the time when an observation is available. This can be represented as follows.

$$\begin{Bmatrix} \mathbf{m}_k^d \\ \mathbf{d}_k \end{Bmatrix} = f(\mathbf{m}_{k-1}^s, \mathbf{m}_{k-1}^d) \text{.....} \quad (3)$$

where *f* represents simulation from time *k-1* to time *k*. Note that the static variables like permeability and porosity do not change in the forecast step. The forecast step is followed by the update step whereby the state variables are updated using the Kalman update equation as follows[18,19]

$$\boldsymbol{\Psi}_k^u = \boldsymbol{\Psi}_k^p + \mathbf{K}\left(\mathbf{D}_k - \mathbf{H}\boldsymbol{\Psi}_k^p\right) \text{.....} \quad (4)$$

The superscript *u* denotes updated and *p* denotes prior. Here, the matrix **K** is the Kalman gain and the matrix **D** represents an ensemble of sampled observations, both defined later. The measurement matrix **H** just selects the calculated production response from the state vector and is a trivial matrix given below.

$$\mathbf{H} = \begin{bmatrix} \mathbf{0} & \mathbf{I} \end{bmatrix} \text{.....} \quad (5)$$

where **I** is the identity matrix. The Kalman gain matrix is computed as follows[18,19]

$$\mathbf{K} = \mathbf{C}_\Psi^p \mathbf{H}^T \left(\mathbf{H}\mathbf{C}_\Psi^p \mathbf{H}^T + \mathbf{C}_D\right)^{-1} \text{.....} \quad (6)$$

where $\mathbf{C}_\Psi^p$ represents the state vector covariance matrix and $\mathbf{C}_D$ represents the observation covariance matrix. The ensemble of sampled observations $\mathbf{D}_k$ can be represented as follows

$$\mathbf{D}_k = \{\mathbf{d}_{k,1} \quad \mathbf{d}_{k,2} \quad \ldots \quad \mathbf{d}_{k,N_e}\} \quad \ldots\ldots\ldots\ldots\ldots\ldots\ldots\ldots\ldots (7)$$

$$\mathbf{d}_{k,i} = \mathbf{d}_k + \boldsymbol{\varepsilon}_i \quad \ldots\ldots\ldots\ldots\ldots\ldots\ldots\ldots\ldots\ldots\ldots\ldots\ldots (8)$$

where $\mathbf{d}_k$ represents a vector of production data measured at time *k*, perturbed by the data noise $\boldsymbol{\varepsilon}_i$ assumed to be Gaussian and uncorrelated in time.

Because the true state vector is not known, we approximate it with the mean of the ensemble. Then the covariance matrix $\mathbf{C}_\Psi^p$ can be estimated at any point in time.

$$\overline{\mathbf{y}}^p = \frac{1}{N_e}\sum_{i=1}^{N_e}\mathbf{y}_i^p \quad \ldots\ldots\ldots\ldots\ldots\ldots\ldots\ldots\ldots\ldots\ldots\ldots (9)$$

$$\mathbf{C}_\Psi^p = \frac{1}{N_e - 1}\sum_{i,j=1}^{N_e}(\mathbf{y}_i^p - \overline{\mathbf{y}}^p)(\mathbf{y}_j^p - \overline{\mathbf{y}}^p)^T \quad \ldots\ldots\ldots\ldots\ldots (10)$$

Because the vector **y** contains both the model parameters **m** and the measurements **d**, the covariance matrix can be re-expressed as

$$\mathbf{C}_\Psi^p = \begin{bmatrix} C_{mm} & C_{md} \\ C_{dm} & C_{dd} \end{bmatrix} \ldots\ldots\ldots\ldots\ldots\ldots\ldots\ldots\ldots\ldots\ldots (11)$$

Thus, the full covariance matrix consists of four sub-matrices which are defined below

$$\mathbf{C_{mm}} = \mathbf{E}\left[(\mathbf{m} - \overline{\mathbf{m}})(\mathbf{m} - \overline{\mathbf{m}})^\mathbf{T}\right] \ldots\ldots\ldots\ldots\ldots\ldots\ldots\ldots (12)$$

$$\mathbf{C_{md}} = \mathbf{C_{dm}} = \mathbf{E}\left[(\mathbf{m} - \overline{\mathbf{m}})(\mathbf{d} - \overline{\mathbf{d}})^\mathbf{T}\right] \ldots\ldots\ldots\ldots\ldots\ldots (13)$$

$$\mathbf{C_{dd}} = \mathbf{E}\left[(\mathbf{d} - \overline{\mathbf{d}})(\mathbf{d} - \overline{\mathbf{d}})^\mathbf{T}\right] \ldots\ldots\ldots\ldots\ldots\ldots\ldots\ldots\ldots (14)$$

In the Kalman gain equation the covariance matrix in **Eq. 10** can be computed, but is not necessary. In fact, the measurement matrix **H** selects only certain sub-matrices within the entire state-vector covariance, specifically the cross-covariance terms and the data covariances. Thus, in practice there is no need to compute the full covariance matrix, which can be extremely time-consuming. Recognizing the fact that $\mathbf{C_{md}}$ is the cross-covariance between the data and model parameters, we propose to condition this matrix using the streamline-derived analytic sensitivities, which define a region of influence of the data.

We weight the terms in the cross-covariance matrix by a weighting function determined from the streamline-derived sensitivities. The covariance matrix is redefined as

$$\mathbf{C}_{\Psi}^{p}\mathbf{H}^{t} = \boldsymbol{\rho} \circ \left(\frac{1}{N_e - 1} \sum_{i,j=1}^{N_e} (\mathbf{y}_i^p - \overline{\mathbf{y}}^p)(\mathbf{H}\mathbf{y}_j^p - \mathbf{H}\overline{\mathbf{y}}^p)^T \right) \quad \text{..... (15)}$$

where the operation ρ° in **Eq. 15** denotes the Schur product operator which is an element-by-element multiplication procedure.[16,17] The term ρ is a weighting function acting as a 'covariance filter' and contains the information extracted from the sensitivities between the predicted flow response and the model parameters. Note that sensitivity-based covariance filter includes flow path information and the relationship between changes in the production response at wells to changes in the model parameters (see **Fig. 3b**).

The weighting function ρ is defined as a matrix with the column *j* (referring to a particular well) containing the weights as shown in **Fig. 3b** for the grid locations *i* as shown in **Fig. 3a.** Wherever the sensitivities are below a threshold cut-off, the weighting function is set to zero. This ensures that erroneously large covariances computed for distant locations without data support are blocked out. Also, using the normalized sensitivities give a smoother transition to the cut-off. We build the weighting function at each assimilation time for each well, thereby creating an area of influence for each measurement weighted by their relative significance.

Sensitivity Computations. We briefly discuss here the streamline-based sensitivity computation for completeness. The details can be found elsewhere.[1,11-14] First, we can compute the streamline travel time or time-of-flight sensitivities analytically as simple integrals along streamlines. For example, the time-of-flight sensitivity with respect to permeability is given by[1]

$$\frac{\partial \tau}{\partial k(\mathbf{x})} = \int_{\Sigma} \frac{\partial s(\mathbf{x})}{\partial k(\mathbf{x})} d\mathbf{x} = -\int_{\Sigma} \frac{s(\mathbf{x})}{k(\mathbf{x})} d\mathbf{x} \quad \text{.............................. (16)}$$

where the integrals are evaluated along streamlines and the 'slowness' which is the reciprocal of interstitial velocity is defined as

$$s(\mathbf{x}) = \frac{\phi(\mathbf{x})}{\lambda_{rt} k(\mathbf{x}) \left| \nabla P(\mathbf{x}) \right|} \quad \text{.................................... (17)}$$

These quantities are available after a forward run of the streamline simulator or can be derived from a finite-difference simulator based on the inter-block fluid fluxes.[15]

Water-Cut Sensitivity. Using the compressible streamline formulation, the sensitivity of the arrival time *t* of a particular water cut for model parameter *m* (permeability in this case) can be defined as[11]

$$\frac{\partial t}{\partial m} = \frac{\dfrac{\partial \tau}{\partial m} \dfrac{\partial}{\partial \tau} \left(\dfrac{S_W}{B_W} \right)}{\dfrac{\partial}{\partial \tau} \left(\dfrac{f_w}{B_w} \right) + \dfrac{f_w}{B_w} \dfrac{c}{\phi}} \quad \text{.............................. (18)}$$

where *c* represents the divergence of flux, $\nabla \cdot \vec{u}_t$ along the streamline and can be computed from the velocity field.. The sensitivity of water-cut at a particular time can then be computed via chain rule.[12]

Gas-Oil Ratio Sensitivity. The sensitivity of the arrival time *t* of a particular value of gas-oil ratio to model parameter *m* can be defined as[11]

$$\frac{\partial t}{\partial m} = \frac{\frac{\partial \tau}{\partial m}\frac{\partial}{\partial \tau}\left(\frac{S_g}{B_g}+\frac{S_o R_s}{B_o}\right)}{\frac{\partial}{\partial \tau}\left(\frac{f_g}{B_g}+\frac{f_o R_s}{B_o}\right)+\left(\frac{f_g}{B_g}+\frac{f_o R_s}{B_o}\right)\frac{c}{\phi}} \quad \text{…….…. (19)}$$

where *c* represents the divergence of flux as before. Again, the sensitivity of gas-oil ratio at a particular time can be obtained by chain rule of differentiation.[12]

The Covariance Filter, ρ. Given these streamline-based sensitivities, we can now populate the matrix ρ. The sensitivities are rescaled to a maximum of one and a minimum of zero. The matrix ρ then contains information about the streamline trajectory and the relative importance of each of the gridblocks to the production response of water-cut or gas-oil ratio. The fact that the covariance localization is flow-relevant is crucial here. The sensitivities ensure that the gridblocks that are adapted are indeed related to the measurements and no unwanted averaging takes place, thereby preserving permeability connectivity.

Errors in the Covariance Matrix and the Effect of Ensemble Size. Following the approach of Hamill and Whitaker[16], we show how errors in the covariance matrix are related to the ensemble size for a simple two-dimensional example. In fact, based on this result, we can infer that the covariance localization used here has similar effects as increasing the ensemble size.

Consider a bi-variate random vector $Z^T=(X, Y)$. An initial realization of this random vector may be denoted by $z_p^T=(x_p, y_p)$. The covariance matrix P of this random vector can be written as

$$P = \begin{bmatrix} \sigma_1^2 & c_{xy} \\ c_{xy} & \sigma_2^2 \end{bmatrix} \text{……..…….…..... (20)}$$

The error in estimating the covariances between X and Y are related to ensemble size *n* and the true correlation ρ by[16]

$$\text{Error}(\hat{\theta}) \propto \frac{1}{n}(1+\rho^2) \text{……...….....} \quad (21)$$

We can see that an increase in the ensemble size ‘n’ reduces the error in predicting the covariance between the variables, X and Y. We can compare the error in the covariance with the expected value of the covariance and call it the relative error.

$$\text{Relative Error} = \frac{\text{Error}(\hat{\theta})}{c_{xy}} \propto \frac{1}{n}\frac{(1+\rho^2)}{\rho} \quad \text{.....(22)}$$

Fig. 7 shows how the error in the covariances varies with ensemble size and with the coefficient of correlation. The results are intuitive. With increasing correlation, the second variable Y is predicted with less uncertainty or with less variance in the predicted estimate. Thus, the effect of a covariance estimation error is reduced with greater correlation between the variables. As the correlation decreases, the relative magnitude of the error is higher, and the prediction variance of the estimate is also higher, consequently, the errors increase. With a larger set of realizations of the random vector, it is possible to obtain an estimate of the true covariance with lesser inaccuracies, hence the error decreases. The covariance localization attempts to reduce the error by keeping ρ high within the region of influence.

Application and Discussion

We demonstrate the application and advantages of the Conditioned EnKF using two examples. First, we use the benchmark SPE-9 case to illustrate the applicability for general three-phase flow conditions.[11] Next, we illustrate the practical feasibility of our proposed approach using a field example that involves integrating 20 years of water-cut data.

The SPE-9 Example. The SPE-9 test case was used to demonstrate the application of the Conditioned EnKF to a 3- phase example. An ensemble of 60 realizations for the permeability field was generated geostatistically using the well data.20 One of the realizations was used as a reference case and the water-cut and gas-oil ratio corresponding to this permeability field was used as observed measurements. For flow simulation, we used the commercial streamline simulator FRONTSIM®.

We history matched the water-cut and GOR response using the standard EnKF and the Conditioned EnKF. The total production history was available for a period of 900 days. We assimilated production data for 570 days, every 60 days. Next, using the updated models at the end of 570 days, we forecast the production response for the next 330 days.

Fig. 8 shows a comparison of the initial and updated gas-oil ratio and water cut for the Conditioned EnKF. We can see that within the specified noise tolerances, the technique is capable of matching the observed history for the first 570 days. The next 330 days is the prediction interval and as expected, the spread in the predictions from different ensemble members is considerably reduced after assimilating the production data. It is worth mentioning here that similar performance was also observed from the standard EnKF for this example.

The advantages of the covariance localization for the Conditioned EnKF can be seen after analyzing the final permeability maps. **Fig. 9** compares the updated permeabilities for one realization from the standard and conditioned EnKF techniques. As can be seen the standard EnKF tends to cause permeabilities to overshoot and to create localized patches of high and low permeabilities. Moreover, the updated field does not seem to be consistent with the initial model. However, with the conditioned EnKF, the updated permeabilities are more consistent with the prior model and honor the geologic information present in the initial model. We also do not observe any overshooting of permeability at any location.

The Goldsmith Field Case. We now discuss the application of the standard EnKF to a field case and compare the results with the Conditioned EnKF. The field case is from the Gold Smith San Andres Unit GSAU, a dolomite formation in west Texas. The pilot area in Fig. 10 consists of nine inverted five-spot patterns covering approximately 320 acres with an average thickness of 100 ft. The area has 20 years of waterflood production history before the initiation of the CO2 project in 1996. The study area includes 11 injectors and 31 producers. Production history information from 9 producers is used because only these have significant water cut response. The detailed production rate and the well schedule, including infill drilling, well conversions, and well shut-in can be found elsewhere.14 The study area was discretized into 58x53x10 grid blocks. The initial 50 realizations of porosity and permeability were obtained using sequential Gaussian co-simulation conditioned to well and seismic data. Fig. 11a shows one of the initial realizations. Notice that the permeability histogram is non-Gaussian with multi-modal features.

Using the standard EnKF, we conditioned the ensemble of realizations to the water-cut history. **Fig. 11b** shows one of the ensemble members after a sequence of updates. Notice that the permeability distribution is now completely Gaussian. The standard EnKF was unable to preserve the initial multimodal nature of the permeability histogram leading to loss of geologic structure in the permeability field. In addition, initially the ensemble members have permeabilities ranging from 0.005 md to 500 md. After assimilating the water-cut data, the updated permeabilities range between $1.6x10^{-5}$ md and $1.8x10^{5}$ md. Others have also observed such overshooting/undershooting problems.[4-6]

Next, we use the conditioned EnKF to update the realizations to honor the production data. The permeability field in **Fig. 11c** is the result of using our covariance localization scheme. Clearly, we are able to preserve the multimodal character of the permeability distribution. The water-cut matches are shown in **Fig. 12** and the conditioned EnKF performs quite well in matching production data. The same kind of match was also obtained using the standard EnKF.

Fig. 13 shows the cross-covariance between the water-cut at a particular well and the permeabilities in the rest of the field for a certain time step. With the unconditioned standard EnKF with a limited ensemble size, the covariance matrix can be seen to be noisy and there is a strong, but inaccurate, relation to distant grid blocks. However, this is not the case with the Conditioned EnKF where the support is more localized and the effect of distant grid blocks has been reduced. Thus, the changes are minimized and targeted by the production response. This is why we are able to preserve much of the character of the initial permeability distribution.

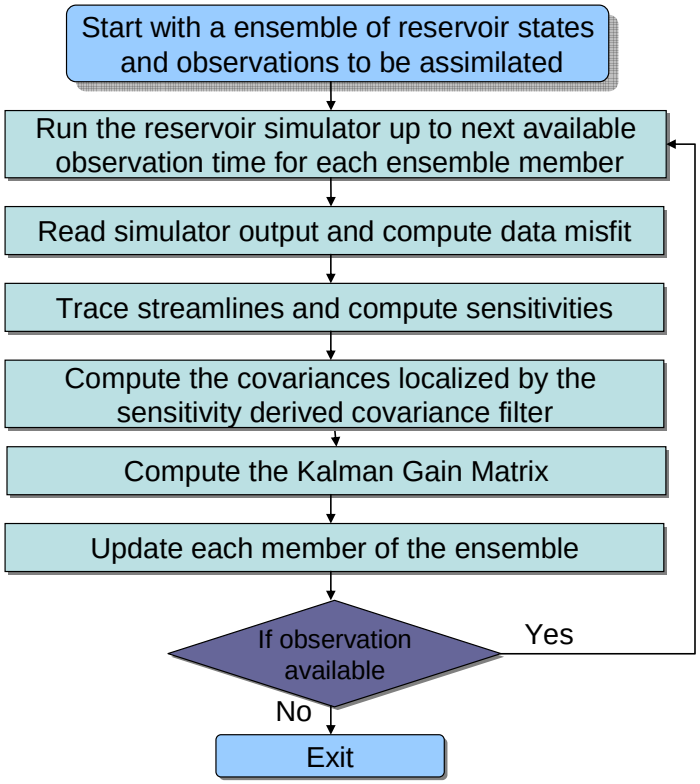

Figure 1. Algorithm for the Conditioned EnKF. The conditioning step appears only when computing the Kalman Gain Matrix.

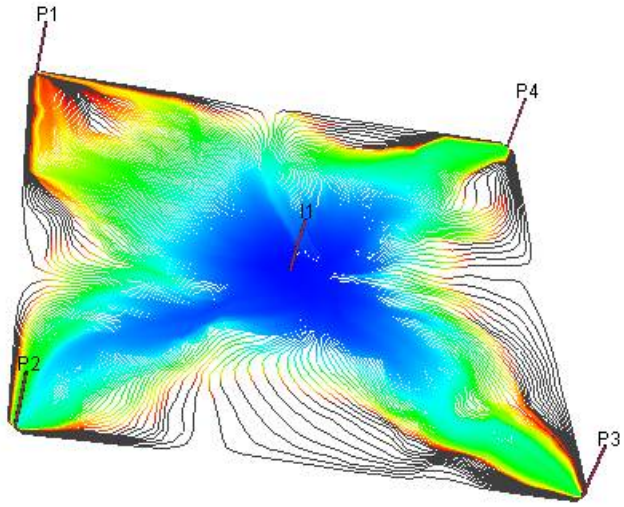

Figure 2. Streamlines and the Time-Of-Flight throughout the field for the reference model.

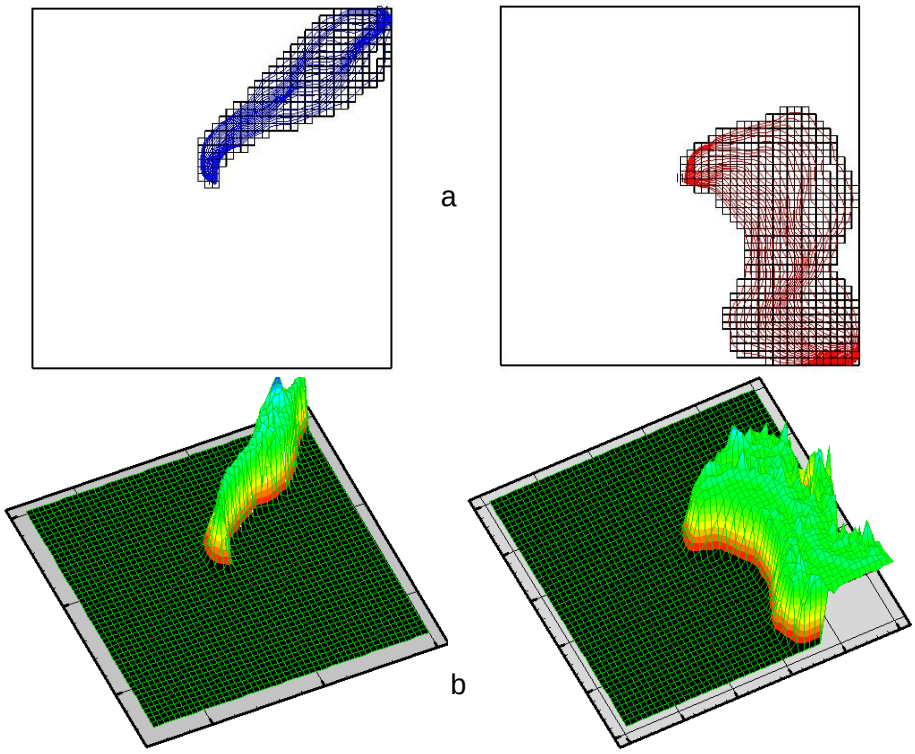

Figure 3. The streamline trajectory and the normalized streamline-derived analytic sensitivities to water-cut for two wells for a selected realization in the ensemble.

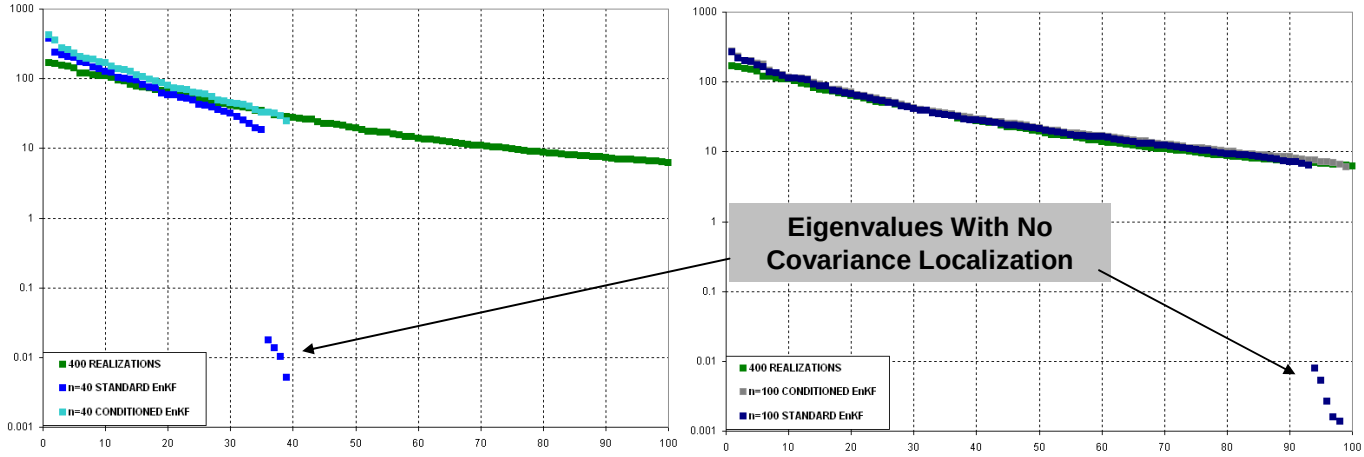

Figure 4. The Eigenvalue spectrum for different ensemble sizes. The 400-member ensemble is assumed to be representing the true spectrum. Reducing the ensemble size tends to degrade the eigenvalue spectrum. However, with covariance localization, the tendency to have reduced variance in the trailing eigen-directions is mitigated.

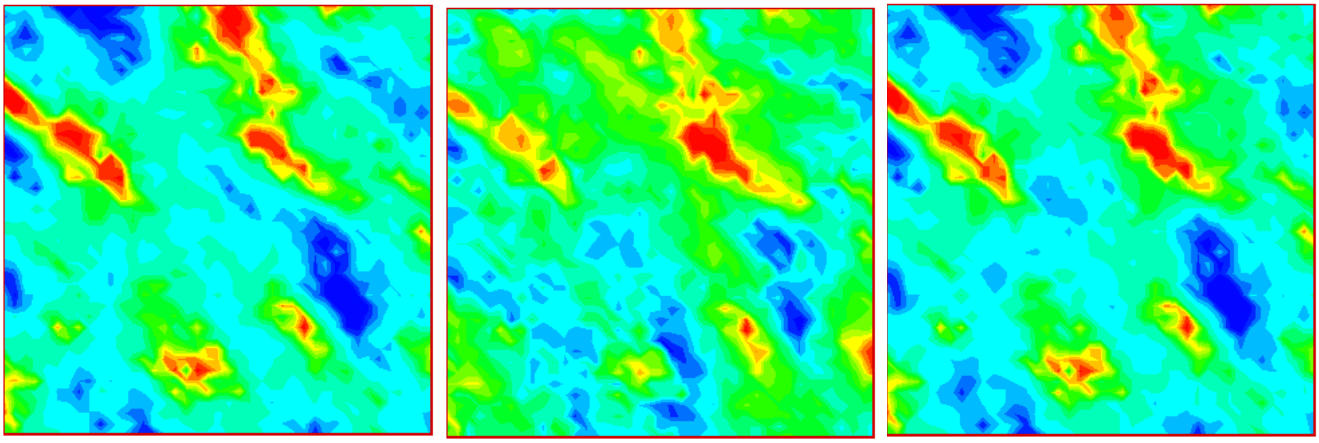

a **b**

c

Figure 5. The resultant log-permeability fields for one realization. (a) is the initial model, (b) is the final permeability field obtained from the Standard EnKF and (c) is from the Conditioned EnKF. The permeability fields were conditioned to water-cut data from the reference field.

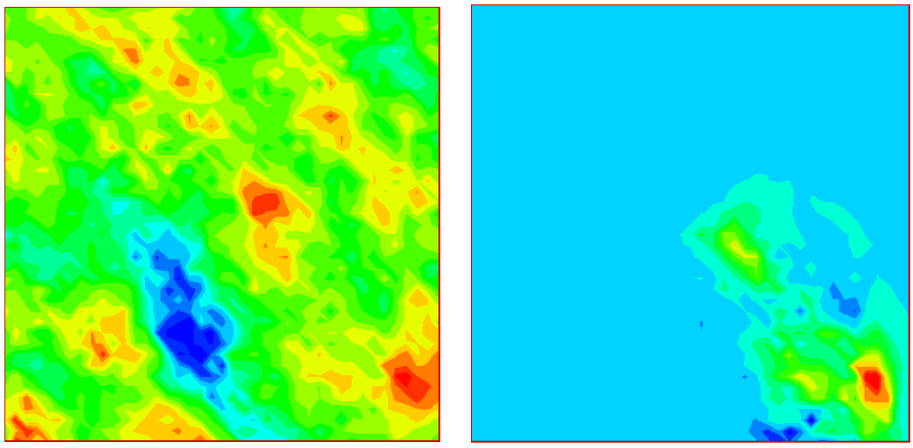

a **b**

Figure 6. The cross-covariance between water-cut and permeability at a certain time for one well computed for an ensemble size of 40. (a) shows the cross-covariance computed from the ensemble, (b) is the cross-covariance computed from the ensemble and conditioned using the sensitivities

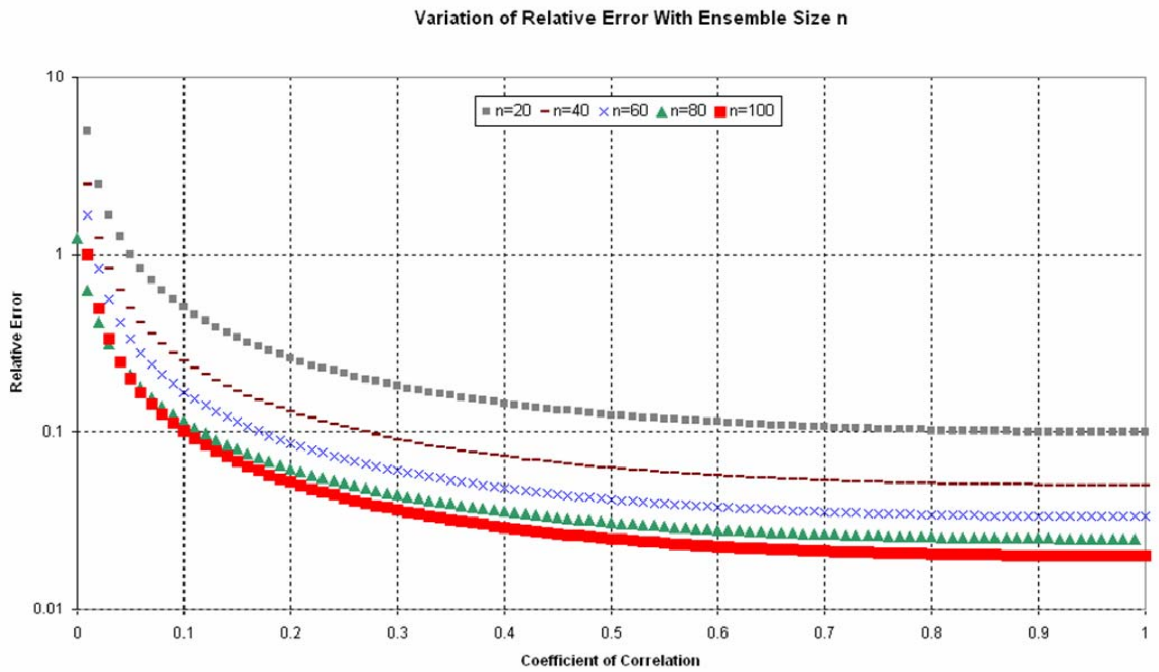

Figure 7. Variation of the error in the cross-covariance with ensemble size and the coefficient of correlation. Notice that even with a high correlation, the relative error is large for small ensemble sizes emphasizing the need for covariance localization.

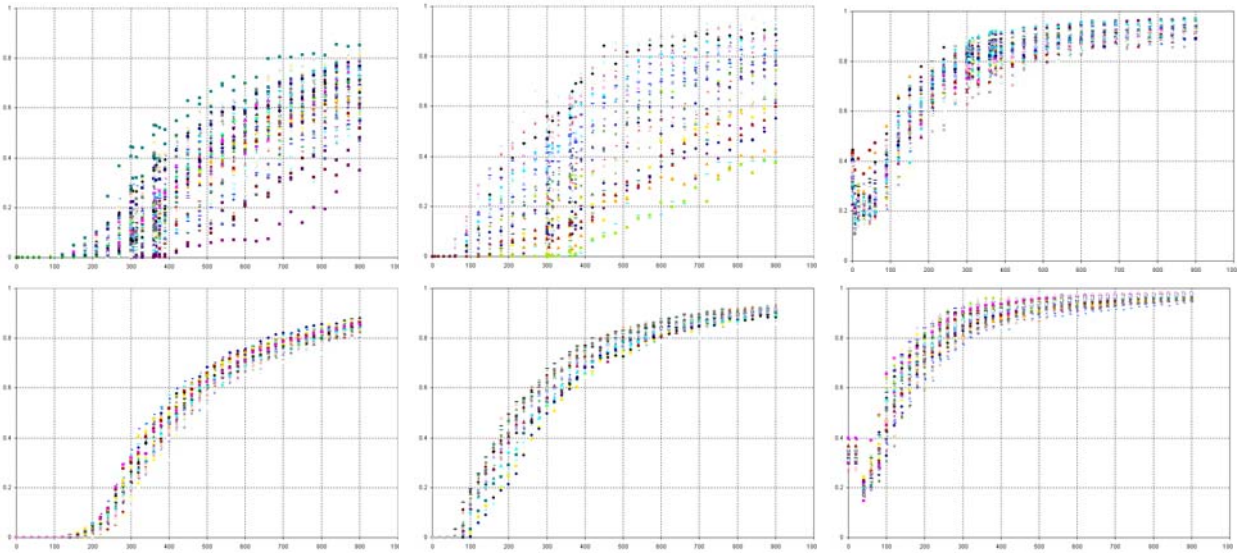

Figure 8a. The water-cut for 3 sample wells showing the initial water-cut spread at the top and the history matched water-cut at the bottom for the corresponding wells. The history match was performed for 570 days and predictions run for the next 330 days.

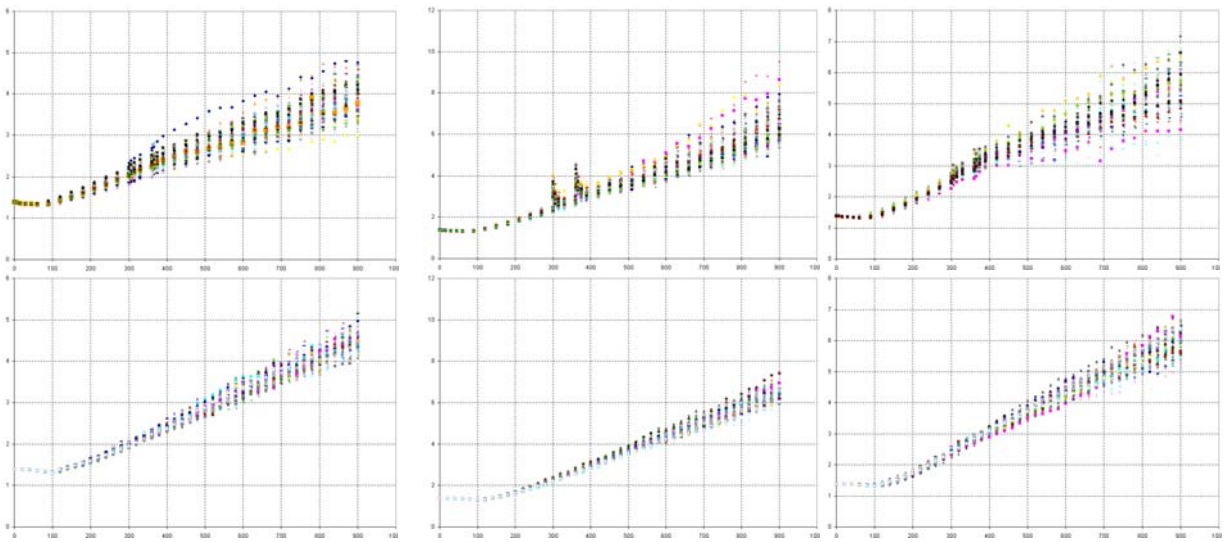

Figure 8b. The GOR for 3 sample wells. The initial GOR spread is at the top and the final history matched GOR at the bottom. The history match was performed for 570 days and predictions run for the next 330 days.

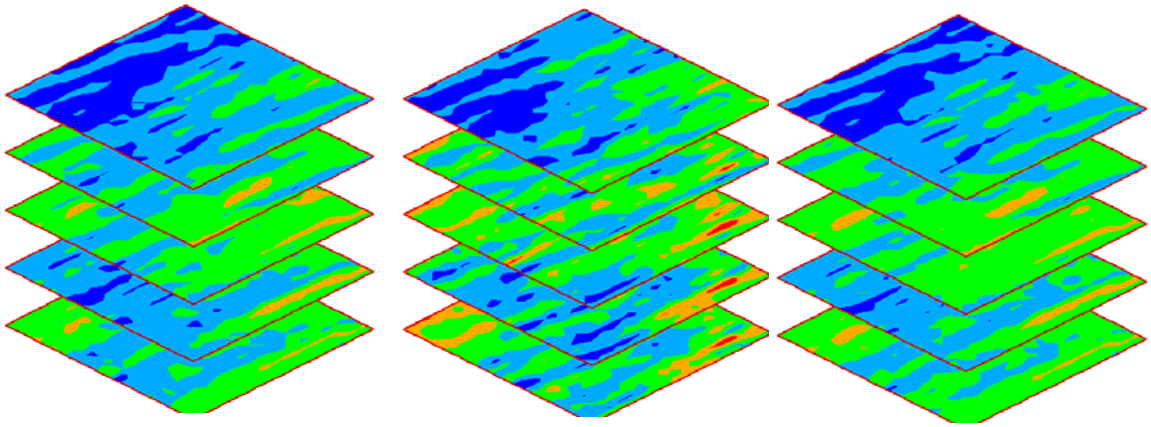

a **b**

c

Figure 9. Comparison of the initial and updated permeability for one representative ensemble member. (a) Initial model (b) Updated using the standard EnKF (c) Updated using the conditioned EnKF

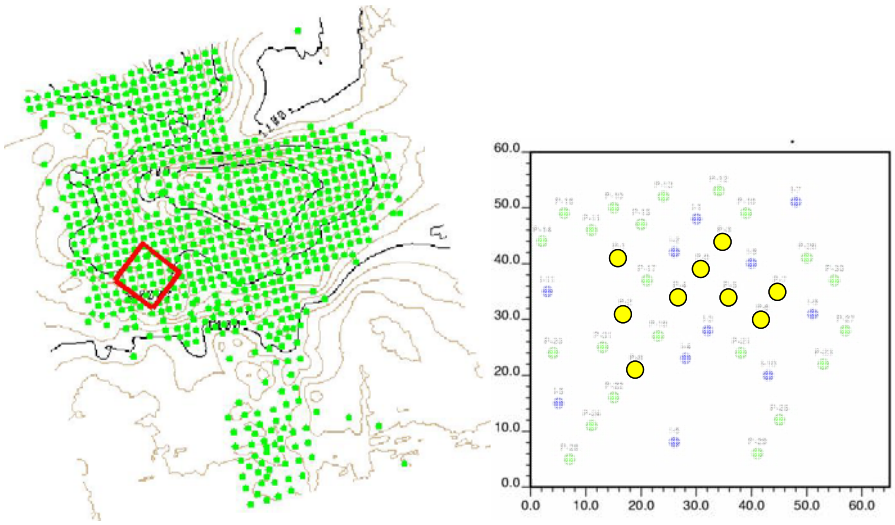

Figure 10. Goldsmith study area; 9 producers with water cut data highlighted in yellow; Injectors in blue (from He and Datta-Gupta.[14])

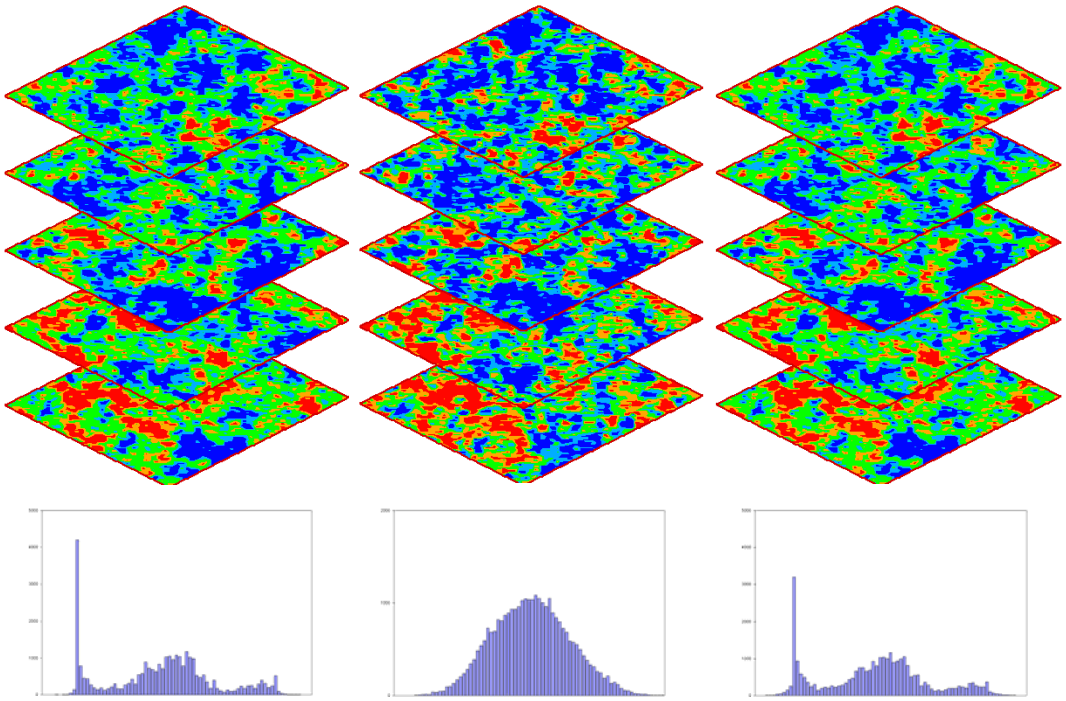

a: Initial Model **b: Updated Model, Standard EnKF** **c: Updated Model, Conditioned EnKF**

Figure 11. The updated permeabilities for the Standard EnKF and the Conditioned EnKF and the respective log-permeability histograms.

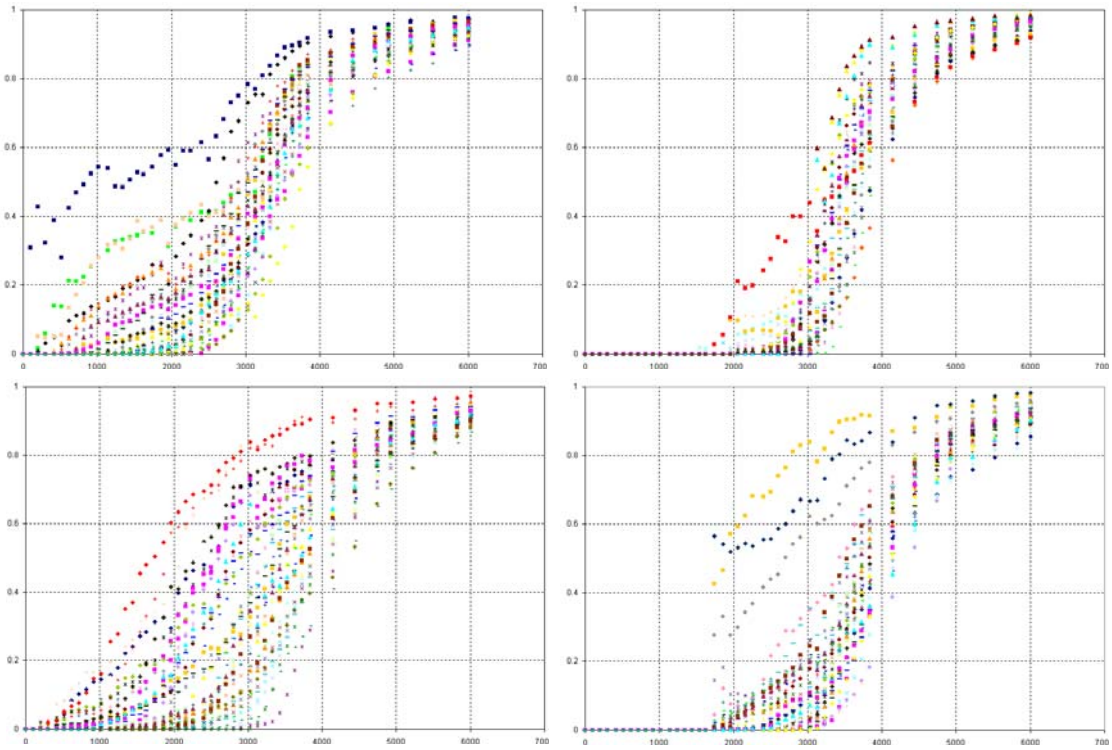

Figure 12a. The initial water-cut at four of the wells in the field for 50 ensemble realizations

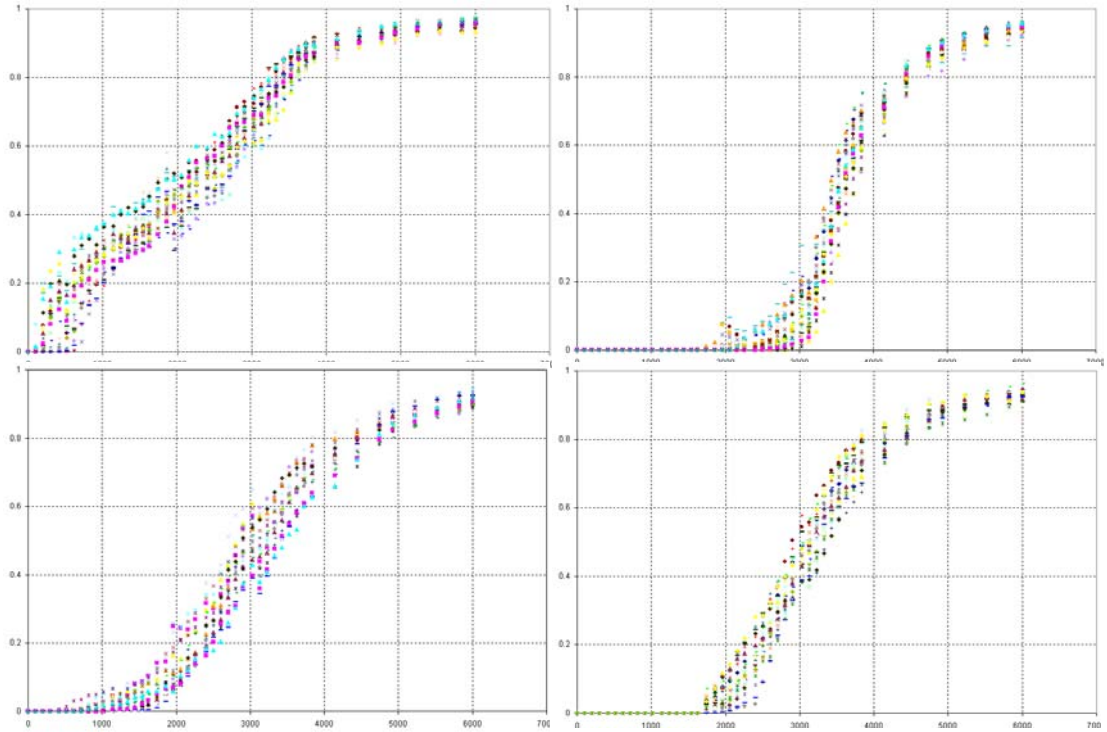

Figure 12b. The matched water-cut at four of the wells in the field for 50 ensemble realizations.

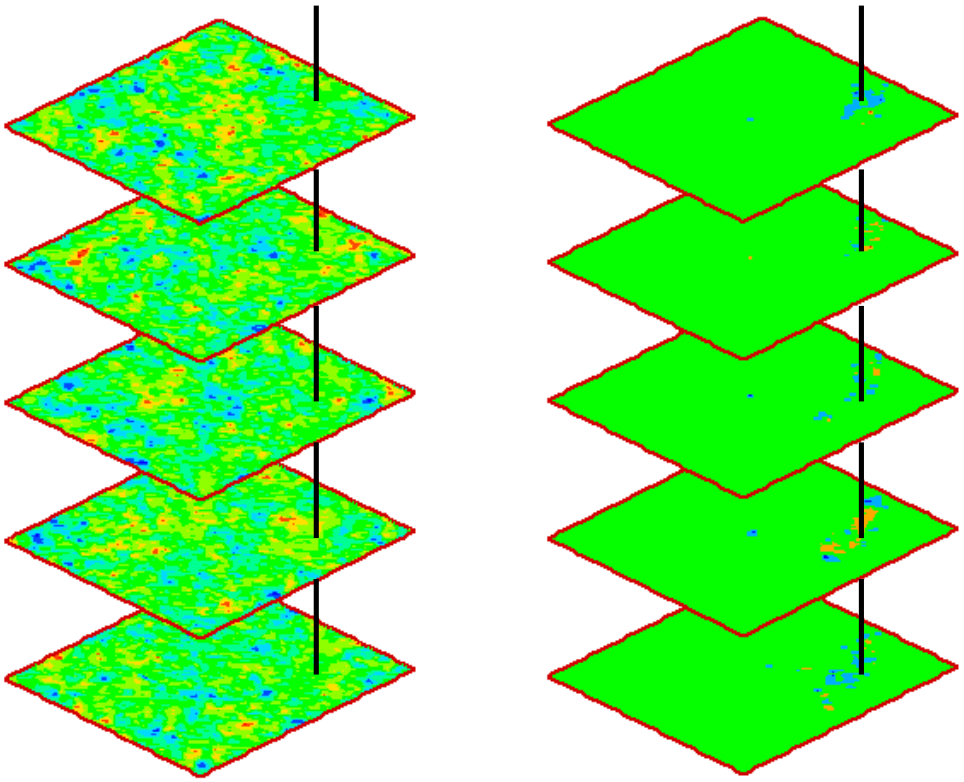

a **b**

Figure 13. The cross-covariance computed between the water-cut at a well and the permeabilities in the field. (a) shows the cross-covariance using 50 ensemble members with the Standard EnKF and (b) shows the same for the Conditioned EnKF. Note how the effect of distant data points has been reduced or eliminated using streamline-derived sensitivity conditioning.

CONCLUSIONS

Part-I

A computationally efficient and practical approach to history matching three-phase flow data is presented. We have validated the technique by applying it to both synthetic and field cases. The importance of a pressure match in any three-phase production integration has been emphasized and in our application, we have combined the streamline technique for water-cut and GOR arrival time match with low-frequency asymptotic method for pressure inversion in reconciling geologic model to three-phase production data. To facilitate the travel time inversion of the non-monotonic GOR data, we present a transformation of the production data and provide the appropriate streamline-based sensitivities for data inversion. Some specific conclusions are summarized below.

- We have presented a method for history matching three-phase flow that involves simultaneous inversion of water-cut, GOR and bottom-hole flowing pressure data. Whereas the water-cut and GOR related sensitivities are obtained using the streamline-based approach, we have used a low frequency asymptotic approach for computing the pressure sensitivities.
- The effectiveness of the generalized travel time inversion is demonstrated using synthetic and field examples. We have shown that a simple transformation of the production data makes it much more amenable to the application of the GTTI.
- Although we have not explicitly accounted for pressure in our saturation sensitivity formulation, we have incorporated the zero frequency component of a low-frequency asymptotic approach to pressure inversion into our workflow while preserving the efficiency of the streamline-based inversion. The seamless incorporation of pressure inversion in our workflow ensures a simultaneous match on water-cut, GOR and pressure.
- The practical applicability of our proposed approach has been demonstrated by its application to synthetic and field cases.

Part-II

We have presented an enhancement to the standard EnKF by utilizing parameter sensitivities to localize the covariance matrix. Our approach uses streamline-based sensitivities from the selective flow path information and weights the cross-covariance matrix using a covariance filter. The approach avoids much of the problems associated with standard EnKF related to parameter overshoots and loss of geologic realism during history matching. The synthetic example and the field applications presented demonstrate the practical utility and robustness of our approach. Some specific conclusions are summarized below.

- The use of streamline-derived analytic sensitivities for covariance localization mitigates and reduces some of the reported problems in the use of the EnKF related to overshooting of the

reservoir parameters and the loss of geologic realism for strongly non-linear problems or non-Gaussian distributions, particularly for practically feasible ensemble sizes for field applications (50~100).

- The ability of the Conditioned EnKF to retain the shape of the non-Gaussian nature of the histograms lends to a more reasonable updated model, which retains spatial continuity and reproduces the flow barriers and flow channels. This key feature improves the quality and confidence of the forecasts from the history-matched models since they are consistent with geologic information.
- Our approach can also lead to a significant saving in computational effort. We have shown that in order to realize the same benefits of our proposed covariance localization, the standard EnKF would require a significantly larger ensemble size. This can make the approach computationally very expensive, particularly for field scale applications.

REFERENCES

Part-I

1. Vasco, D.W., Yoon, S., and Datta-Gupta, A.: "Integrating Dynamic Data Into High-Resolution Reservoir Models Using Streamline-Based Analytic Sensitivity Coefficients," SPE Journal (December 1999) 389.
2. Datta-Gupta, A. et al.: "Streamlines, Ray Tracing and Production Tomography: Generalization to Compressible Flow," Petroleum Geoscience (May 2001), 75.
3. Reis, L.C., Hu, L.Y., and Eschard, R.: "Production Data Intergration Using a gradual Deformation Approach: Application to an Oil Field (Offshore Brazil)" paper SPE 63064 Presented at the 2000 Annual Technical Conference and Exhibition, Dallas, Texas, 1-4 October.
4. Landa, J.L., Kamal, M.M., Jenkins, C.D., and Horne, R.N.: Reservoir Characterization Constrained to Well Test Data: A Field Example," paper SPE 36511, Presented the 1996 SPE Annual Technical Conference and Exhibition, Denver 6-9 October.
5. Anterion, F., Karcher, B., and Eymard, .R. "Use of parameter gradients for reservoir history matching," paper SPE 18433, Presented at the 1989 SPE symposium on reservoir simulation, Houston 6-8 February.
6. Wu, Z., Reynolds, A. C., and Oliver, D.S.: "Conditioning Geostatistical Models to Two-Phase Production Data" SPE Journal, 4(2), 142-155, June (1999).
7. Wang, Y. and Kovscek, A.R.: "A Streamline Approach to History Matching Production Data," paper SPE 59370 presented at the 2000 SPE/DOE Symposium on Improved Oil Recovery, Tulsa, 3-5 April.
8. Sahni, I., and Horne, R.: Multiresolution Wavelet Analysis for Improved Reservoir Description". SPE Reservoir Evaluation & Engineering, February, 53-69, (2005)
9. Cheng, H. et. al.: "Compressible Streamlines and Three-Phase History Matching, " paper SPE 99465 presented at the 2006 SPE/DOE Symposium on Improved Oil Recovery, Tulsa, 22-26 April.
10. He, Z., Datta-Gupta, A., and Yoon, S.: "Streamline-Based Production Data Integration with Gravity and Changing Field Conditions," SPE Journal, 7(4), 423-436, December (2002).
11. Vasco, D.W. and Karasaki, K.: "Interpretation and inversion of low-frequency head observations," Water Resour. Res (2006) 42., W05408
12. Paige, C.C and Saunders, M.A.: "LSQR: An Algorithm for Sparse Linear Equations and Sparse Least Squares," ACM Trans. Math. Software (1982) 8, No. 1, 43
13. Bear, J., 1972. Dynamics of Fluids in Porous Media. Dover Publications, Inc., New York, 764pp
14. Vega, L, Rojas, D., and Datta-Gupta, A.: "Scalability of the Deterministic and Bayesian Approaches to Production-Data integration Into Reservoir Models." SPE Journal (September 2004) 330.
15. Killough, J.E.: "Ninth SPE Comparative Solution Project: A Reexamination of Black-Oil Simulation," paper SPE 29110 presented at the 13th SPE Symposium on Reservoir Simulation held in San Antonio, TX, 12-15 February 1995.

Part-II

1. Vasco, D.W., Yoon, S., and Datta-Gupta, A.: "Integrating Dynamic Data Into High-Resolution Reservoir Models Using Streamline-Based Analytic Sensitivity Coefficients," SPE Journal (December 1999) 389.

A. S. Emanuel and W. J. Milliken "History Matching Finite Difference Models with 3D Streamlines," paper SPE 4900 presented at the 1998 SPE Annual Technical Conference and Exhibition, New Orleans 27-30 September.

2. Sen, M., Datta-Gupta, A., Stoffa, P., Lake, L. W. and Pope, G. A., "Stochastic Reservoir Modeling Using Simulated Annealing and Genetic Algorithm," SPE Formation Evaluation, 10 (1), 49-55, 1995.
3. Gu, Y., Oliver, D.S.: "The Ensemble Kalman Filter for Continuous Updating of Reservoir Simulation Models," J. of Energy Resources Technology (March 2006), 128 pp 79.
4. Gu, Y., Oliver, D. S.: "History Matching of the PUNQ-S3 Reservoir Model Using the Ensemble Kalman Filter," paper SPE 89942 presented at the 2004 Annual Technical Conference and Exhibition, Houston 26-29 September.
5. Nævdal, G. et al.: "Reservoir Monitoring and Continuous Model Updating Using Ensemble Kalman Filter," paper SPE 84372 presented at the 2003 Annual Technical Conference and Exhibition, Denver, 8-5 October.
6. Gao, G., Zafari, M., and Reynolds, A.C. : "Quantifying Uncertainties for the PUNQ-S3 Problem in a Bayesian Setting With RML EnKF," paper SPE 93324 presented at the 2002 Improved Oil Recovery Symposium, Tulsa, Oklahoma 13-17 April.
7. Zafari, M., Reynolds, A.C.: "Assessing the Uncertainty in Reservoir Description and Performance Prediction With the Ensemble Kalman Filter," paper 95750 presented at the 2005 Annual Technical Conference and Exhibition, Dallas, 9-12 October.
8. Skjervheim, J.A. et at: "Incorporating 4D Seismic Data in Reservoir Simulation Model Using Ensemble Kalman Filter," paper 95789 presented at the 2005 Annual Technical Conference and Exhibition, Dallas, 9-12 October.
9. Elkin-Arroyo, Deepak Devegowda, and Akhil Datta-Gupta. "Streamline Assisted Ensemble Kalman Filter for Rapid and Continuous Reservoir Model Updating," paper SPE 104255 presented at the 2006 SPE Internation Oil and Gas Conference, Beijing, China, 5-7 December.
10. Cheng. H. et al.:"Compressible Streamlines and Three-Phase History Matching," paper SPE 99465 presented at the 2006 SPE/DOE Symposium on Improved Oil Recovery, Tulsa, Oklahoma, U.S.A., 22-26 April.
11. Hao Cheng. et al: "A Comparison of Travel-Time and Amplitude Matching for Field-Scale Production Data Integration: Sensitivity, Non-Linearity and Practical Implications Filter," SPE Journal (March 2005) 75.
12. Cheng, H. et al.: "Fast History Matching of Finite-difference Models Using Streamline-derived Sensitivities," SPE Reservoir Evaluation and Engineering, 8 (5), October 2005, p426-436.
13. He, Zhong and Datta-Gupta, A. "Streamline-based Production Data Integration Under Changing Field Conditions," SPE Journal, (December 2002), 7 (4).

14. E. Jimenez, et al.: “Spatial Error and Convergence in Streamline Simulation,” paper 92873-MS presented at the 2005 Reservoir Simulation Symposium, 31 January-2 Feburary, The Woodlands, Texas.
15. Hamill, T.M., Whitaker, J.S.: “Distance-Dependent Filtering of Background Error Covariance Estimate in an Ensemble Kalman Filter,” J. Monthly Weather Review 2001, 129 pp 2776.
16. Houtekamer, P.L. and Mitchell, H.L.: “A Sequential Ensemble Kalman Filter for Atmospheric Data Assimilation,” J. Monthly Weather Review 2001, 129 pp 123.
17. Evensen, G.: “Sequential Data Assimilation with a Nonlinear Quasi-Geostrophic Model Using Monte Carlo Methods to Forecast Error Statistic,” J. of Geophysical Research, (1994), 162, 143.
18. Evensen, G.: “The ensemble Kalman filter: Theoretical formulation and practical implementation,” Ocean Dynamics, 53:343–367, 2003.
19. Deutsch, C.V., Journel, A., 1992, GSLIB Geostatistical Software Library and User’s Guide, Oxford U. Press.

LIST OF ACRONYMS AND ABBREVIATIONS

Part-I

B_o, B_w, B_g = *formation volume factor, Oil, Water, Gas*
c = divergence of total flux
f_o, f_w, f_g = *fractional flow, Oil, Water, Gas*
k = permeability
k_{ro}, k_{rw}, k_{rg} = *relative permeability, Oil, Water, Gas*
k_{rog} = *relative permeability to oil (oil-gas-connate water)*
K_{row} = *relative permeability to oil (oil-water)*
M = reservoir parameter
P = pressure
P_o=*zero-th order pressure amplitude*
$\hat{P}$ =*zero frequency pressure component*
q_o, q_w, q_g = *volumetric flux, Oil, Water, Gas*
Q_o, Qw, Qg = *production rate, Oil, Water, Gas*
R_s = *solution gas oil ratio*
S_o, S_w, S_g = *saturation, Oil, Water, Gas*
t = time
$\vec{u}$ = *total Darcy velocity*
τ = *time of flight*
ϕ = *porosity*
ρ = *effective density*
ψ, χ = *bi-streamfunctions*
μ_o, μ_w, μ_g = *viscosity, Oil, Water, Gas*
λ_t = *total mobility*

Part-II

$\mathbf{y}_k^p$ =Prior model-parameter state vector, at time k
$\bar{\mathbf{y}}^p$ = Mean of the prior model-parameter state vector
$\mathbf{m}_k^s$ = Static variable vector at time k
$\mathbf{m}_k^s$ = Dynamic variable vector at time k
$\mathbf{d}_k$= Observed or calculated data
K= Kalman gain
$\mathbf{D}_k$ = Ensemble observation at time k

H = Measurement matrix

$\mathbf{C}_{\Psi}^{p}$ = State vector covariance matrix

$\mathbf{C}_{\Psi}^{p}\mathbf{H}^{t}$ = Model data cross covariance matrix

$\mathbf{H}\mathbf{C}_{\Psi}^{p}\mathbf{H}^{t}$ = Calculated data covariance matrix

$\mathbf{C}_{D}$ = Data observation covariance matrix

N_e = Number of members in the ensemble

$\mathbf{\Psi}_k$ = Ensemble of state vectors

$\boldsymbol{\varepsilon}_i$ = White random noise data observation

ρ = Correlation function

τ = Streamline time of flight

ϕ = Porosity

S_o, S_w, S_g=Saturation, Oil, Water, Gas

f_o, f_w, f_g=Fractional Flow, Oil, Water, Gas

B_o, B_w, B_g=Formation Volume Factor, Oil, Water, Gas

National Energy Technology Laboratory

626 Cochrans Mill Road
P.O. Box 10940
Pittsburgh, PA 15236-0940

3610 Collins Ferry Road
P.O. Box 880
Morgantown, WV 26507-0880

One West Third Street, Suite 1400
Tulsa, OK 74103-3519

1450 Queen Avenue SW
Albany, OR 97321-2198

539 Duckering Bldg./UAF Campus
P.O. Box 750172
Fairbanks, AK 99775-0172

Visit the NETL website at:
www.netl.doe.gov

Customer Service:
1-800-553-7681